

SOIL SALINITY IN ARID NON-FLOODED RIPARIAN AREAS

by

Sung-ho Hong

Submitted in partial fulfillment
of the requirement for the degree of
Master of Science in Hydrology

December, 2002

New Mexico Institute of Mining and Technology
Department of Earth and Environmental Science
Socorro, New Mexico

ABSTRACT

Soil salinity is a common problem in arid riparian areas of the arid Southwest, but the dynamics of soil salinity in these areas are not well understood. The main causes of soil salinity in non-flooded riparian areas are generally known as low precipitation, high evapotranspiration, and capillary flux from saline shallow ground water. However, some riparian areas maintain a relatively low soil salinity for a long period of time with thriving salt-sensitive vegetation such as Cottonwoods while other areas are completely salinized and covered by salt-tolerant vegetation such as Saltcedars. Is this difference in soil salinity caused by a small amount of deep infiltration sufficient to leach salts back to the ground water or by ground water dynamics that “wash” the soil profile from below? The results of this study, using the modeling program HYDRUS-1D, indicate that soil salinity is a complex process affected by a number of factors such as soil profile texture, ground water table depth and its fluctuation, ground water quality, and time period of simulation. First, a validation of the HYDRUS-1D model demonstrated that predicted apparent soil electrical conductivities of six representative soil profiles show a good correlation with the apparent soil electrical conductivities measured in the field with the Geonics EM38 ground conductivity meter. A sensitivity analysis was conducted to analyze which factors determine soil salinity under the riparian conditions of my study area. Soil texture—which determines capillary rise—is the most important predictor

variable for long term soil salinity; generally finer soil texture leads to more saline soils in this environment due to higher capillary rise. The effect of deep infiltration on soil salinity was examined. Differences in soil salinity levels among different riparian areas are not caused by a small amount of deep infiltration but by ground water fluctuations that “wash” the soil profile from below. Although evapotranspiration affects the rate of soil salinization over time, the basic processes of soil salinity have not been changed.

ACKNOWLEDGEMENTS

I would like to express my sincere gratitude to Dr. Jan Hendrickx for his guidance, advice, and helpful discussions during both the research and writing phases of this study. I would also like to thank my other committee members, Drs. Eric Small and Brian Borchers for their advice and encouragement during my research.

I wish to acknowledge Drs. Bruce Harrison and Jirka Simunek, and graduate students Ben Moayyad, Graciela Rodriguez, and Tim Miller for their valuable support in a number of ways. I also would like to thank my wife Youn-A and my parents for their support during my master's program.

This research was funded by the U.S. Fish and Wildlife Service and by SAHRA- Sustainability of semi-Arid Hydrology and Riparian Areas, a NSF Science and Technology Center (STC).

All of you helped out in ways that made my research more bearable and productive.

TABLE OF CONTENTS

	Page
ABSTRACT	
ACKNOWLEDGEMENTS	ii
LIST OF TABLES	v
LIST OF FIGURES.....	vii
1. INTRODUCTION.....	1
2. METHODS AND MATERIALS	5
2.1 Study Area	5
2.2 Field Measurements	6
2.3 Laboratory Measurements.....	7
2.4 HYDRUS-1D Model.....	9
Boundary and initial conditions	12
2.5 Soil Salinity Modeling in Representative Profiles.....	14
2.6 Sensitivity Analysis.....	14
2.7 Soil Salinity Estimation.....	21
Electrical conductivity calculation.....	21
Modeling response of EM38 ground conductivity meter.....	23
Temperature effect	27

3. RESULTS AND DISCUSSION	30
3.1 Characterization of the Representative Soil Profiles	30
3.2 Soil Salinity Modeling in Representative Profiles.....	35
3.3 Sensitivity Analysis.....	45
3.4 Soil Salinity in Arid Riparian Areas in the Middle Rio Grande Valley	51
3.5 Effect of Evapotranspiration on Soil Salinity.....	59
4. CONCLUSIONS.....	66
REFERENCES.....	68

LIST OF TABLES

	Page
TABLE 1. Van Genuchten model parameters for sensitivity analysis	17
TABLE 2. Maximum capillary rise (cm) for ten fluxes in homogeneous loamy sand and loam soil profiles using the Van Genuchten parameters in Table 1	19
TABLE 3. Sensitivity analysis schedule, showing the high (+) and low (-) level of the five parameters for each design point	20
TABLE 4. Field characteristics of the six representative soil profiles.....	31
TABLE 5. Soil stratigraphy and Van Genuchten model parameters for the six representative soil profiles.....	33
TABLE 6. Model Feddes' root uptake parameters	36
TABLE 7. Results of the sensitivity analysis, showing the outcome of each scenario in terms of the total amount of soluble salts in the rootzone (220 cm).....	48
TABLE 8. Main effects of soil texture, average ground water depth, ground water fluctuation amplitude, time of simulation, and depth model domain factors on the total amount of the soluble salts in the rootzone (220 cm) TSS_{root}	50
TABLE 9. Capillary fluxes entering the rootzone from the ground water table for the six representative profiles at three constant ground water levels and with three rootzone thicknesses. Roots have uniform distribution throughout rootzone	52
TABLE 10. Total amount of soluble salts [g / (220 or 500 cm ³)] accumulated in the representative profiles after simulations using current ground water TDS values.....	54

TABLE 11. Total amount of soluble salts [g / (220 or 500 cm³)] in the representative profiles after simulations with 200 ppm ground water quality56

TABLE 12. Comparison between modeled and SEBAL evapotranspiration and crop coefficient 63

LIST OF FIGURES

	Page
FIGURE 1. Schematic of the root-water stress response function, $\alpha(h)$ after Feddes et al. (1978)	11
FIGURE 2. Schematic of the model for layered soil conductivity profiles. d is the thickness of the soil layer, σ is the apparent electrical conductivity, μ is the magnetic permeability, h is the height, and M is the number of layers	25
FIGURE 3. Mean soil temperature profile during January 1999, calculated using Eqs. [33]–[34]	29
FIGURE 4. Root density function of Saltcedar and Cottonwood (maximum density = 1)	34
FIGURE 5. Soil stratigraphy and texture of representative profiles 1 and 2 with the profile of the water content, soil-salt content, and soil-water concentration after 30 years in the 5 m model domain depth and ground water table depth (mean, high, and low). Initial ground water and time-independent bottom solute boundary conditions are 200 ppm (SIL: silty loam, SL: sandy loam, S: sand, L: loam, LS: loamy sand, CS: coarse sand)	37
FIGURE 6. Soil stratigraphy and texture of representative profiles 3 and 4 with the profile of the water content, soil-salt content, and soil-water concentration after 30 years in the 5 m model domain depth and ground water table depth (mean, high, and low). Initial ground water and time-independent bottom solute boundary conditions are 200 ppm (SC: sandy clay, C: clay, CL: clay loam)	38
FIGURE 7. Soil stratigraphy and texture of representative profiles 5 and 6 with the profile of the water content, soil-salt content, and soil-water concentration after 30 years in the 5 m model domain depth and ground water table depth (mean, high, and low). Initial ground water and time-independent bottom solute boundary conditions are 200 ppm (SCL: sandy clay loam, SI: silt)	39
FIGURE 8. Total amount of the salt (Top) and mean soil-water concentration (Bottom) in the rootzone over time (initial ground water and time-independent bottom solute boundary conditions are 200 ppm, 5 m model domain depth)	40

FIGURE 9. The soil-water solute concentration profiles after 30 and 60 years in the 5 m model domain depth (Profiles 1–3: Cottonwood, Profiles 4–6: Saltcedar)	42
FIGURE 10. The soil-water solute concentration profiles after 30 and 60 years in the 20 m model domain depth (Profiles 1–3: Cottonwood, Profiles 4–6: Saltcedar)	43
FIGURE 11. Comparison between modeled and measured apparent electrical conductivity of soil in 5 m soil profile (dotted square shows the range of EM38 field measurement).....	46
FIGURE 12. Comparison between modeled and measured apparent electrical conductivity of soil in 20 m soil profile	47
FIGURE 13. Salt distribution profiles during period without infiltration events in Profile 1 (start: 17280 day, end: 17320 day)	60
FIGURE 14. Salt distribution profiles during the wettest season (top) and during the major infiltration event (bottom) in Profile 1.....	61
FIGURE 15. Solute concentration profiles using observed and uniform root distribution after 30 years in the model depth (bottom solute boundary condition: 200 ppm).....	65

This thesis is accepted on behalf of the
faculty of the Institute by the following committee.

Adviser

Date

I release this document to the New Mexico Institute of Mining and Technology.

Student's Signature

Date

1. INTRODUCTION

In an arid environment with a shallow ground water table, soil salinity occurs because evapotranspiration exceeds rainfall, and capillary rise allows salts to accumulate in the rootzone and near the soil surface.

In general, soil with a salt concentration more than 2,500 ppm is considered a saline soil (White, 1997). The origins of salts in soil and water are chemical weathering of minerals, atmospheric deposition, saline ground water tables, irrigation water, soil amendments, and fertilizers (Hanson et al., 1993). Mineral weathering is the most dominant process that affects the chemistry of waters in rivers, soils, and shallow ground water. It involves the dissolution, alteration, and precipitation of minerals and for the most part takes place in the soil aeration zone. Atmospheric deposition is also a salt source. Sterling (2000) documented that the amount of atmospheric chloride deposition in the Midwest U.S. is about 0.1 g/m^2 per year.

The presence of salt in a soil causes an increase in the osmotic potential of the soil-water. This, in turn, may stress many plants, which severely affects the survival rates of crop species (Hussain et al., 1994). The major impact of salt on the hydraulic properties of soil is that sodium reduces the infiltration rate which is attributed to dispersion of clays into the soil pores, surface crusting, and swelling of clay (Brady et al., 1999). This may cause poor soil aeration and have a negative impact on the plant growth. Therefore, soil salinity is an important factor during revegetation efforts in riparian areas.

A number of previous studies have identified factors that affect water and solute movement in the vadose zone. Childs et al. (1975) concluded that the salt concentration in soil with a shallow ground water table depends on the physical characteristics of the soil, ground water table depth, and rooting depth of the plant. Torres et al. (1989) noticed a direct relationship between capillary rise and crop evapotranspiration. They calculated the contribution of ground water table depth (50, 100, and 150 cm) to crop evapotranspiration (ET) in a silty clay loam and a sandy loam soil and concluded that ET increased with shallower ground water table depth. Kruse et al. (1993) also mentioned that the presence of a saline shallow ground water table is a major contributor to accumulation of salts in the rootzone. Hendrickx et al. (1997) researched soil salinity and its effect on revegetation potential along the Rio Grande between Las Cruces and El Paso and showed that salt accumulation resulted from capillary rise of ground water and lack of leaching. Silliman et al. (2001) conducted laboratory experiments using homogeneous and heterogeneous porous media to investigate the effect of capillary fringe on water and solute transport. They documented that the capillary fringe played an important role in water flux and solute transport in both vertical and horizontal flow directions.

Numerous numerical models have been developed for simulating water flow and solute transport through the vadose zone. Prathaper et al. (1992) applied the LEACHC model to estimate capillary rise from a saline shallow ground water table. The total salt increment within the profile was calculated by multiplying the salt concentration in the ground water table by the cumulative capillary rise. Other examples of numerical models are SWAP (Work Group SWAP, 1996), VAM2D (Huyakorn et al., 1989), SWMS-2D (Simunek et al., 1994), and HYDRUS-1D (Simunek et al., 1998).

Most soil salinity studies deal with the salt balance of irrigated agricultural fields. Soil salinity is kept relatively low by applying an excess of irrigation water to leach salts accumulated in the rootzone back to the shallow ground water. The salts in the ground water are removed by a subsurface drainage system. Thus, in irrigated agriculture soil salinity is managed by inducing a downward water flux which leaches salts well below the rootzone into the shallow aquifer.

Riparian areas along the Rio Grande in arid New Mexico are characterized by patches of saline and non-saline soils. Some riparian sites in the middle Rio Grande Basin are exposed to infrequent flooding and may maintain a favorable salt balance by soil leaching. However, after the construction of dams and flood protection measures in the 20th century, most riparian areas are never exposed to flooding. Therefore, it is not clear why some soils with shallow ground water tables maintain a relatively low salinity level for long periods of time while others become very saline within a few years.

It is well understood why under these riparian conditions soil salinity is occurring at so many locations in the riparian Rio Grande Valley. Salts and water are transported toward the rootzone by capillary rise from the shallow ground water, the water is used by the vegetation, and salts accumulate in the rootzone. If soil salinity increases, vegetation changes from salt-sensitive Cottonwoods to salt-tolerant Saltcedar and salt grasses. In the end, soil salinity will increase to such a level that no more vegetation can exist.

It is not well understood why some sites in the non-flooded riparian areas of the Rio Grande maintain a relatively low soil salinity with thriving salt-sensitive vegetation. Is this caused by a small amount of deep infiltration sufficient to leach salts back to the ground water or by ground water table dynamics that “wash” the rootzone from below?

The answer to this question is critical for the future management of New Mexico's arid riparian areas.

The objectives of this thesis are (1) to validate the model HYDRUS-1D (Simunek et al., 1998) for prediction of long term soil salinity in the arid riparian areas of the middle Rio Grande, (2) to use HYDRUS-1D for evaluation of the key factors causing riparian soil salinity, and (3) to answer the question of whether a small amount of excess rainfall or ground water table dynamics keep some riparian rootzones salt free.

2. METHODS AND MATERIALS

2.1 Study Area

The fieldwork for this study was conducted in a riparian area near the city of Albuquerque in New Mexico. My research sponsor prefers to remain anonymous and has requested that I do not include the geographical coordinates of the study sites. However, I will provide all data needed to repeat and verify the results and conclusions of this study.

The climate at Albuquerque is arid to semi-arid, with an average annual air temperature of 15°C. Summer daily temperatures range from 20 to 40°C, while winter daily temperatures range from -12 to 10°C. Mean annual precipitation is about 25 cm and mean annual potential evapotranspiration is approximately 170 cm.

The vegetation of the study area is native trees, Cottonwoods (*Populus fremontii*) and Willows (*Salix*), and non-native vegetation, Saltcedar (*Tamarix chinensis*) and Russian Olive (*Elaeagnus angustifolia*). In this study, the dominant species of Cottonwood and Saltcedar were selected to study soil salinity.

2.2 Field Measurements

A detailed salinity survey was conducted in January 1999 using the Geonics EM38 ground conductivity meter (Geonics Limited, Mississauga, Ontario) (Hendrickx et al., 1997, 2002). More than 2,000 measurements of the apparent soil electrical conductivity were made over an area of 4 km². In this study I used electromagnetic (EM) measurements taken within a 30 m radius from the representative soil profiles.

The depth to the ground water table has been measured in 19 observation wells since 1997. Nineteen ground water samples were collected in July 1999 to measure total dissolved solids (TDS) and electrical conductivity using the New Mexico Bureau of Mines and Mineral Resources Chemistry Laboratory. Soil stratigraphy and texture data were determined from three representative soil pits by visual and/or tactile analysis. Root distribution data in both Cottonwood and Saltcedar areas were collected from two soil pits by visual observations. The root-density profiles were obtained by counting roots on two walls 100 cm wide by 220 cm deep with count weights defined as: <2 mm diameter = 1 count; 2 to 4 mm = 2 counts; 4 to 10 mm = 3 counts; >1 cm = diameter (mm)x5 counts.

Daily precipitation data from 1970 to 1999 at the Albuquerque International Airport, New Mexico, were obtained from the National Climate Data Center Online (<http://lwf.ncdc.noaa.gov/oa/ncdc.html>). The daily potential evapotranspiration (ET₀) rates were calculated using the Penman-Monteith Equation during 1995 to 1999 from weather data measured at the Rio Grande Nursery weather station in Albuquerque, New Mexico.

2.3 Laboratory Measurements

Three soil pits were dug to identify representative horizons. Undisturbed soil samples were obtained from seven representative stratigraphic units to measure soil hydraulic properties. First, an acrylic column (15 cm diameter and 25 cm length) was pushed into the soil while removing the soil around the outside of the column. The top and bottom of the column were covered with aluminum foil and transported to the laboratory. Then mesh cloth was secured at the bottom of the sample. Each sample was gradually saturated from the bottom to prevent air entrapment. When fully saturated, tensiometers and time domain reflectometry (TDR) probes were installed at 6, 12, and 18 cm below the top of the sample.

TDR probes were used to measure the soil dielectric constant using the TDR cable tester (Tektronix 1502B). The dielectric constants were converted into volumetric water contents using the calibration curve of Topp et al. (1980). The tensiometers used in this study were constructed using a commercial standard 1-bar porous ceramic cup connected to an elbow-shaped nylon fitting and acrylic tube. It was sealed at the top by a rubber stopper. The soil-water pressure was measured using a tensiometer (U.S. Patent No: 4520657, Soil Measurement Systems) (Marthaler et al., 1983; Hendrickx, 1990).

The water-retention curves of each sample were determined by taking simultaneous volumetric water content and soil-water pressure measurements during drying by evaporation of the soil sample.

The measurements were plotted, and the points were fitted to water-retention curves using the Van Genuchten (1980) equations:

$$\theta(h) = \theta_r + \frac{\theta_s - \theta_r}{\left[1 + |\alpha h|^n\right]^m} \quad m = 1 - 1/n \quad [1]$$

$$K(\theta) = K_s \left[\frac{\theta - \theta_r}{\theta_s - \theta_r} \right]^l \left[1 - \left[1 - \left(\frac{\theta - \theta_r}{\theta_s - \theta_r} \right)^{1/m} \right]^m \right]^2 \quad [2]$$

where θ is water content (L^3L^{-3}), θ_s is saturated water content, θ_r is residual water content, h is soil-water pressure (L), α , n , and m are Van Genuchten parameters that determine the shape of the water-retention curve, l is the pore-connectivity parameter (-), K is the unsaturated hydraulic conductivity (LT^{-1}), and K_s is the saturated hydraulic conductivity (LT^{-1}).

The Van Genuchten soil hydraulic parameters (θ_r , θ_s , α , and n) were obtained from a solver algorithm (Microsoft Excel) by using Eq. [1]. The hydraulic conductivity curve was obtained using the fitted parameters θ_r , θ_s , α , and n with the measured saturated hydraulic conductivity in Eq. [2]. During parameter fitting, θ_r was constrained to be less than or equal to 0.1, and the other parameters α , θ_s , and n were constrained to be greater than or equal to 0.

2.4 HYDRUS-1D Model

Numerical models are used to simulate water flow, solute transport, and root water uptake in the subsurface for a variety of applications in research and soil-water management. In this study, I used HYDRUS-1D which is a Microsoft-Windows-based simulation code for modeling one-dimensional water, heat, solute movement, and root water uptake in a variably saturated soil.

The water flow model in HYDRUS-1D uses the Richard's Equation which is solved by the linear finite element/finite difference method. The water flux model uses the following equation for water flow and water mass balance:

$$\frac{\partial \theta}{\partial t} = \left(\frac{\partial}{\partial x} \right) \left[K \left(\frac{\partial h}{\partial x} + 1 \right) \right] - S(\theta(h), r, T_p) \quad [3]$$

where

$$K(h, x) = K_s(x) K_r(h, x), \quad [4]$$

x is the vertical dimension (L), r is the root density function, T_p is the potential transpiration rate (LT^{-1}), S is the root-water uptake sink term (T^{-1}), and K_r is the relative hydraulic conductivity (-).

The root-water uptake model is incorporated into the water flow model by adding a sink term to the Richard's Equation. Each depth in the soil profile is assigned a different sink term, which is dependent on the amount of water present, root density, and the potential transpiration. Root-water uptake is transpiration by the vegetation and is

calculated based on the water available at any given node. The sink term is defined by Feddes et al. (1978):

$$S(h) = \alpha(h)S_p \quad [5]$$

where $\alpha(h)$ is the root-water uptake water stress response function (-) and S_p is the potential water uptake rate (T^{-1}). A schematic of the root-water uptake water stress response function is presented in Figure 1. Notice that root-water uptake is zero near saturation ($h > h1$) and below wilting point ($h < h4$). Maximum root water uptake occurs between $h2$ and $h3$.

The solute transport model solves the convection-dispersion transport equation (CDE). The equation is given by

$$\frac{\partial(\theta C)}{\partial t} = \frac{\partial}{\partial x} \left(\theta D \frac{\partial C}{\partial x} \right) - \frac{\partial q C}{\partial x} \quad [6]$$

where

$$\theta D = D_L |q| + \theta D_w \tau_w \quad [7]$$

C is the solute concentration (ML^{-3}), D is the dispersion coefficient in the liquid phase (L^2T^{-1}), q is the Darcian fluid flux density (LT^{-1}), D_L is the longitudinal dispersivity (L) (= 20 cm), D_w is the molecular diffusion coefficient in free water (L^2T^{-1}) (= 0.432 cm^2/day), and τ_w is the tortuosity factor in the liquid phase.

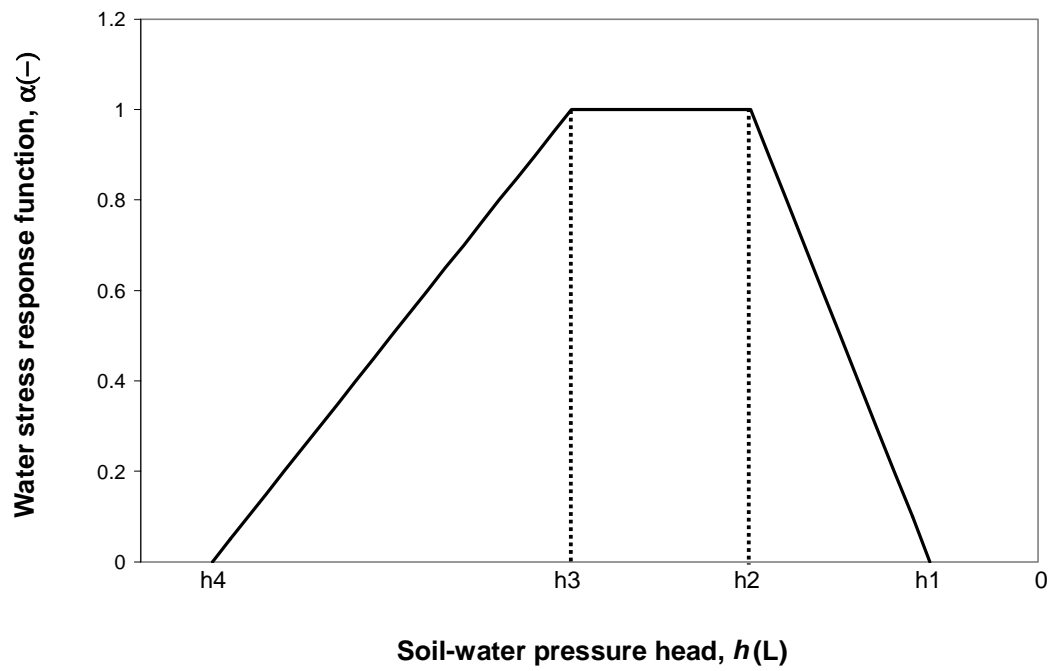


Figure 1. Schematic of the root-water stress response function, $\alpha(h)$ after Feddes et al. (1978).

Boundary and initial conditions: For the simulation of water flux, an atmospheric boundary condition without surface runoff was used as the top boundary and a variable pressure condition was assigned as the bottom boundary condition. The top-water flux boundary condition allows all the water from rainfall to infiltrate into the soil. The variable pressure condition at the bottom boundary makes it possible to assign the ground water table fluctuation. In the models the node spacing varied from 0.1 cm at the surface to 1–3 cm deeper in the profile.

In both the sensitivity analysis and the simulation of representative profiles, a third-type boundary condition was selected as the top boundary condition (Leij et al., 2000). The third-type (Cauchy) boundary condition is defined by:

$$-\theta D \frac{\partial C}{\partial x} + qC = q_0 C_0 \quad \text{at } x = 0 \quad [8]$$

where q is the Darcian fluid flux density (LT^{-1}), q_0 is the water flux boundary condition (LT^{-1}), and C_0 (ML^{-3}) is the concentration of solute in q_0 .

The third-type boundary condition prescribes concentration flux at a boundary, so that the solute concentration flux of water entering or leaving the model domain is fixed by the time-independent solute concentration flux at a boundary. The third-type boundary condition also allows convective and dispersive solute movements but does not have diffusive solute movement caused by diffusion if no convective flux occurs. A combination of second- and third-type boundary conditions was selected in this study as the bottom solute boundary conditions. The second-type (Neumann) boundary condition has the form:

$$\theta D \frac{\partial C}{\partial x} = 0 \quad \text{at } x = 0 \quad [9]$$

where θ is the water content, and D is the dispersion coefficient (L^2T^{-1}).

The second-type boundary condition (zero solute gradients) eliminates dispersive solute movement and only allows convective solute movement at a boundary. The second-type boundary condition at a bottom boundary can be used to simulate solute flux in the deep vadose zone where the ground water table depth is far below the model domain.

The initial solute concentration of the ground water and the time-independent bottom solute boundary condition were set to equal values. For the representative profiles in the simulation, solute concentration at a bottom boundary and initial ground water solute concentrations were 200, 500, 1000, 2000, and current ground water condition (ppm). Those first four values were selected because the salt content of river and well waters in the study area ranged from around 200 to 2000 ppm.

The total solute concentration of typical rain water in New Mexico ranges from 10 to 15 ppm (Popp et al., 1982). In this study, the solute concentration of rain water was assumed to be zero in order to eliminate the effect of soil salinity caused by solute flux from the top boundary. This assumption is not so unrealistic because the amount of rainfall is quite small and rain water concentration is much less than the concentration of the ground water; therefore, the rain water contribution to the salt concentration in the soil profile is negligible. This approach can emphasize the effect of ground water characteristics on soil salinity.

2.5 Soil Salinity Modeling in Representative Soil Profiles

Six representative soil profiles covering the entire range of soil salinity in the study area were selected to simulate soil salinity using HYDRUS-1D. Van Genuchten parameters of soil horizons were obtained from measured value, neural networks (Schaap et al., 1996), or textural classes (Carsel et al., 1988) and were dependent on data availability.

Three soil profiles were located in Cottonwood areas with a relatively low soil salinity and the other three profiles were from the Saltcedar areas with a relatively high soil salinity. The depths of the model domain were 5 and 20 m so that a total of twelve HYDRUS models were constructed to simulate soil salinity conditions. These models ran for 60 years (21,900 days) by using the actual daily 30-year precipitation data and the daily 5-year potential evapotranspiration (ET_0) rate from Albuquerque.

To run 60 years simulation, the 30-year precipitation data were recycled to predict the soil salinity conditions after the first 30 years. The daily ET_0 rate used in the HYDRUS simulation was a one-year series of Julian day averages during 1995 to 1999 and were used over and over up to 60 years.

2.6 Sensitivity Analysis

In the previous section I discussed how I modeled water flow and solute transport in the riparian areas using HYDRUS-1D. Preliminary analyses, literature reports, and field observations indicated that the following five parameters might play a role in the

salinization processes of arid riparian areas: soil texture, average ground water table depth, amplitude of ground water fluctuation, time of simulation, and the removal of salts by the horizontal flux in the shallow aquifer.

I selected two different soil textures with different heights of capillary rise: a loamy sand and a loam. A maximum capillary rise of 0.1 cm/day capillary flux was calculated for the loamy sand and the loam as 32 and 176 cm, respectively. Field observations indicated average ground water table depths of 2 and 3 m with amplitudes from 0 to 1 m. The time of simulation stands for the time period passing by after an important hydrological event in the riparian zone. For example, after the construction of Cochiti Reservoir, the Rio Grande started degrading and ground water tables in the riparian areas declined. Also, due to flood control the fluctuations of the ground water table were expected to be less pronounced. The removal of salts by the shallow aquifer was modeled using a 5-m and 20-m-deep model domain.

In both 5 and 20 m models, the bottom boundary condition was of the second-type when water and salts were leaving the modeling domain but of the third-type when water and salts were entering the model domain. This approach results in net salt removal from the modeling domain which mimics to some extent salt removal by horizontal flow in the aquifer. The reason is that the salt concentration of water leaving the domain is equal to or higher than the salt concentration of water entering into the domain during periods of capillary rise. The latter is always equal to the salt concentration of the ground water. Salt removal and/or addition by this mechanism are expected to occur at a much higher frequency in the 5-m-deep profile than in the 20-m-deep profile. This approach models in a crude manner the effects of salt removal by horizontal fluxes in the shallow

aquifer. The alternative would have been to use a two- or three-dimensional unsaturated/saturated water flow and solute transport model. However, the complexity of such a model would have resulted in very long calculation times. Moreover, the quality and quantity of my field data did not warrant such an approach.

Among the sensitivity analyses, the deepest ground water table depth was 400 cm from the soil surface. In both the loam and loamy sand model domains, the soil texture below 420 cm to the bottom was very coarse sand. Due to the high hydraulic conductivity of the very coarse sand soil in the saturated zone which leads to low resistance to water flow, ground water flow in this layer has only a negligible effect on the water and solute balances of the rootzone. The soil hydraulic parameters used in the sensitivity analyses are presented in Table 1.

Because there were an infinite number of combinations of the five factors in this study, I needed to optimize my simulation efforts in order to obtain maximum information from a minimum amount of simulations. I used the statistics of experimental designs (e.g., Law & Kelton, 2000; Snedecor & Cochran, 1967; Steel & Torrie, 1980) that allowed us to decide before the simulation runs were made, which combination of factors to simulate so that the desired information could be obtained with the least amount of simulation runs. Such an approach was much more efficient than a “trial-and-error” approach in which one runs simulations with unsystematic combinations of factors to see what happens.

The factors of the experimental design were the input variables to the simulation models. The outputs of my simulations were the responses. The response variable for this study was the total amount of the soluble salts in the 2.2-m-deep rootzone after 30 and 60

Table 1. Van Genuchten model parameters for sensitivity analysis.

Soil Texture	θ_r	θ_s	α (cm ⁻¹)	n (-)	K_{sat} (cm/d)	l (-)
Loamy sand ¹	0.057	0.41	0.124	2.28	350.2	0.5
Loam ²	0.000	0.43	0.0207	1.224	57.42	-2.077
Sand ³	0.051	0.38	0.034	4.42	1428.5	0.5

¹Carsel et al. (1988)

²Wösten (1987)

³Neural networks (100 % sand) (Schaap et al., 1996)

years of simulation. This variable was selected since it determined what would happen to the vegetation due to soil salinity.

In this study I opted for a 2^k *factorial design* that required me to choose two levels of each factor and resulted in a total of 2^k simulation runs. The two levels for each factor were chosen so that they represented two opposite conditions such as low height of capillary rise in the loamy sand and a high height of capillary rise in loam soil (Table 2). The factors could be qualitative, such as soil texture, or quantitative, such as depth to ground water. The two levels could neither be too extreme nor too far apart from each other to avoid the possibility of masking important aspects of the transport process under consideration. I considered a total of five factors for this sensitivity analysis (Table 3) which resulted in $2^5 = 32$ different soil salinization scenarios.

The main effects of each factor were then calculated as the average change in the model response as the factor was changed from its “-” level to “+” level while the other four factors were fixed. For example, the main effect of soil texture (factor 1), e_1 , is thus:

$$e_1 = \frac{\sum_{i=1}^{16} R_i - \sum_{j=17}^{32} R_j}{16} \quad [10]$$

where R_i and R_j are the model responses in simulations i and j .

Table 2. Maximum capillary rise (cm) for ten fluxes in homogeneous loamy sand and loam soil profiles using the Van Genuchten parameters in Table 1.

Soil Texture	Capillary Flux (cm/day)									
	3	2	1	0.8	0.6	0.4	0.2	0.1	0.05	0.01
Loamy Sand ¹	16	17	20	21	22	24	28	32	37	51
Loam ²	32	41	60	66	78	95	130	176	234	425

¹Carsel et al. (1998)

²Wösten (1987)

Table 3. Sensitivity analysis schedule, showing the high (+) and low (-) level of the five parameter groups for each design point.

Scenario	Soil texture ¹	Average ground water depth ²	Ground water fluctuation amplitude ³	Time of simulation ⁴	Depth model domain ⁵	Response ⁶
	Factor 1	Factor 2	Factor 3	Factor 4	Factor 5	
1	+	+	+	+	+	R1
2	+	+	+	+	-	R2
3	+	+	+	-	+	R3
4	+	+	+	-	-	R4
5	+	+	-	+	+	R5
6	+	+	-	+	-	R6
7	+	+	-	-	+	R7
8	+	+	-	-	-	R8
9	+	-	+	+	+	R9
10	+	-	+	+	-	R10
11	+	-	+	-	+	R11
12	+	-	+	-	-	R12
13	+	-	-	+	+	R13
14	+	-	-	+	-	R14
15	+	-	-	-	+	R15
16	+	-	-	-	-	R16
17	-	+	+	+	+	R17
18	-	+	+	+	-	R18
19	-	+	+	-	+	R19
20	-	+	+	-	-	R20
21	-	+	-	+	+	R21
22	-	+	-	+	-	R22
23	-	+	-	-	+	R23
24	-	+	-	-	-	R24
25	-	-	+	+	+	R25
26	-	-	+	+	-	R26
27	-	-	+	-	+	R27
28	-	-	+	-	-	R28
29	-	-	-	+	+	R29
30	-	-	-	+	-	R30
31	-	-	-	-	+	R31
32	-	-	-	-	-	R32

¹Soil texture: + = Loam, - = Loamy sand

²Average ground water depth: + = 200 cm, - = 300 cm

³Ground water fluctuation amplitude: + = 100 cm, - = 0 cm

⁴Time of simulation: + = 60 years, - = 30 years

⁵Depth model domain: + = 20 m, - = 5 m

⁶Response: Total amount of soluble salts in the rootzone (g/220 cm³)

2.7 Soil Salinity Estimation

Electrical conductivity estimation: Rhoades et al. (1989) developed a model for the relationship between apparent soil electrical conductivity σ_a (dS/m), electrical conductivity of soil-water σ_w (dS/m), and soil-water content θ under all soil conditions as follows:

$$\sigma_a = \left[\frac{(\theta_{ss} + \theta_{ws})^2 \sigma_{ws} \sigma_{ss}}{\theta_{ss} \sigma_{ws} + \theta_{ws} \sigma_{ss}} \right] + (\theta - \theta_{ws}) \sigma_{wc} \quad [11]$$

where θ_{ss} is the volumetric solid contents, θ_{ws} is the volumetric water content in small pores, σ_{wc} is the electrical conductivity of the soil-water in the large pores, σ_{ws} is the electrical conductivity of the soil-water in the small pores, and σ_{ss} is the average electrical conductivity of the soil particles

One year later, Rhoades et al. (1990) presented four different procedures to estimate parameters in Eq. [11]. In this study, the parameters for σ_a calculation were obtained from their Procedure I.

$$\theta_{ss} = \rho_b / \rho_s \quad [12]$$

$$\theta_{ws} = 0.639\theta + 0.011 \quad [13]$$

$$\sigma_{ss} = 0.023(\%C) - 0.021 \quad [14]$$

$$\rho_b = 1.73 - 0.0067(0.76(\%C) + 27.25) \quad [15]$$

$$SP = 0.76(\%C) + 27.25 \quad [16]$$

where σ_w is the sum of σ_{wc} and σ_{ws} and assuming $\sigma_{wc} = \sigma_{ws}$, ρ_s is the average density of soil particles (2.65 g/cm^3), ρ_b is the bulk density of soil, %C is the clay content percent of the soil, and SP is the saturation percentage.

The solute concentration of soil-water (TDS) was calculated from HYDRUS. In this study, the following formula was used to convert TDS into σ_w at reference temperature of 25°C was used (Hanson et al., 1993).

$$\sigma_w \text{ (dS/m)} = \text{TDS (ppm)} / 740 \quad (\text{if TDS} < 3700) \quad [17]$$

$$\sigma_w \text{ (dS/m)} = \text{TDS (ppm)} / 840 \quad (\text{if } 3700 < \text{TDS} < 7400) \quad [18]$$

$$\sigma_w \text{ (dS/m)} = \text{TDS (ppm)} / 920 \quad (\text{if TDS} > 7400) \quad [19]$$

The following steps show how to obtain σ_a for each soil depth (z):

Step1. Find $\sigma_w(z)$

From HYDRUS-1D obtained soil-water concentration (TDS) for each depth. Converted TDS into σ_w using the following equations (Hanson et al., 1993).

$$\sigma_w \text{ (dS/m)} = \text{TDS (ppm)} / 740 \quad (\text{if TDS} < 3700)$$

$$\sigma_w \text{ (dS/m)} = \text{TDS (ppm)} / 840 \quad (\text{if } 3700 < \text{TDS} < 7400)$$

$$\sigma_w \text{ (dS/m)} = \text{TDS (ppm)} / 920 \quad (\text{if TDS} > 7400)$$

Step2. Find $\theta(z)$

Volumetric water content (θ) for each depth was obtained from HYDRUS-1D.

Step3. Find $\theta_{ss}(z)$

From Procedure I of Rhodes et al. (1990)

$$\rho_b = 1.73 - 0.0067(0.76 \%C + 27.25)$$

$$\rho_s = 2.65$$

$$\theta_{ss} = \rho_b / \rho_s$$

Step4. Find $\theta_{ws}(z)$

$$\theta_{ws} = 0.639\theta + 0.011$$

Step5. Find $\sigma_{ss}(z)$

$$\sigma_{ss} = 0.023(\%C) - 0.021$$

Step6. Find $\sigma_a(z)$

From Eq. [11] (Rhodes et al., 1989)

$$\sigma_a = \left[\frac{(\theta_{ss} + \theta_{ws})^2 \sigma_{ws} \sigma_{ss}}{\theta_{ss} \sigma_{ws} + \theta_{ws} \sigma_{ss}} \right] + (\theta - \theta_{ws}) \sigma_{wc}$$

Modeling response of EM38 ground conductivity meter: The estimated average soil apparent electrical conductivity of every 10 cm chunk in the soil profile was converted to soil apparent electrical conductivity measured on the soil surface by using a non-linear forward model. This non-linear model predicted the response of the EM38 ground conductivity meter for given conductivities at depths of 5 cm, 15 cm, 25 cm, ..., 305 cm (31 conductivities in all).

Hendrickx et al. (2002) presented and compared linear and non-linear models to predict soil apparent electrical conductivity. They concluded that the linear model

produced twice as many errors as non-linear model. The layered model for soil conductivity profiles and electromagnetic ground conductivity meter measurements at different heights are illustrated in Figure 2. The following series of equations of the non-linear forward model were used in this study to predict the response of the EM38 ground conductivity meter.

In the following equations, the variables λ and g (related by $\lambda = gB/r$) have no physical meaning and were used as the variables of integration in the Hankel transforms. The characteristic admittance of the k^{th} layer is N_k which is defined by:

$$N_k = \frac{\sqrt{\lambda^2 + i\sigma_{ak}\mu_k\omega}}{i\mu_k\omega} \quad [20]$$

where ω is the angular operating frequency of the instrument, σ_{ak} is the apparent electrical conductivity of the k^{th} layer, and μ_k is the magnetic permeability of the k^{th} layer. The surface admittance at the top of the k^{th} layer, Y_k , was calculated from the following set of equations where d is the thickness of the layers:

$$Y_1 = N_1 \frac{Y_2 + N_1 \tanh(u_1 d_1)}{N_1 + Y_2 \tanh(u_1 d_1)} \quad [21]$$

$$Y_2 = N_1 \frac{Y_3 + N_2 \tanh(u_2 d_2)}{N_1 + Y_2 \tanh(u_2 d_2)} \quad [22]$$

$$Y_{M-2} = N_{M-2} \frac{Y_{M-1} + N_{M-2} \tanh(u_{M-2} d_{M-2})}{N_{M-2} + Y_{M-1} \tanh(u_{M-2} d_{M-2})} \quad [23]$$

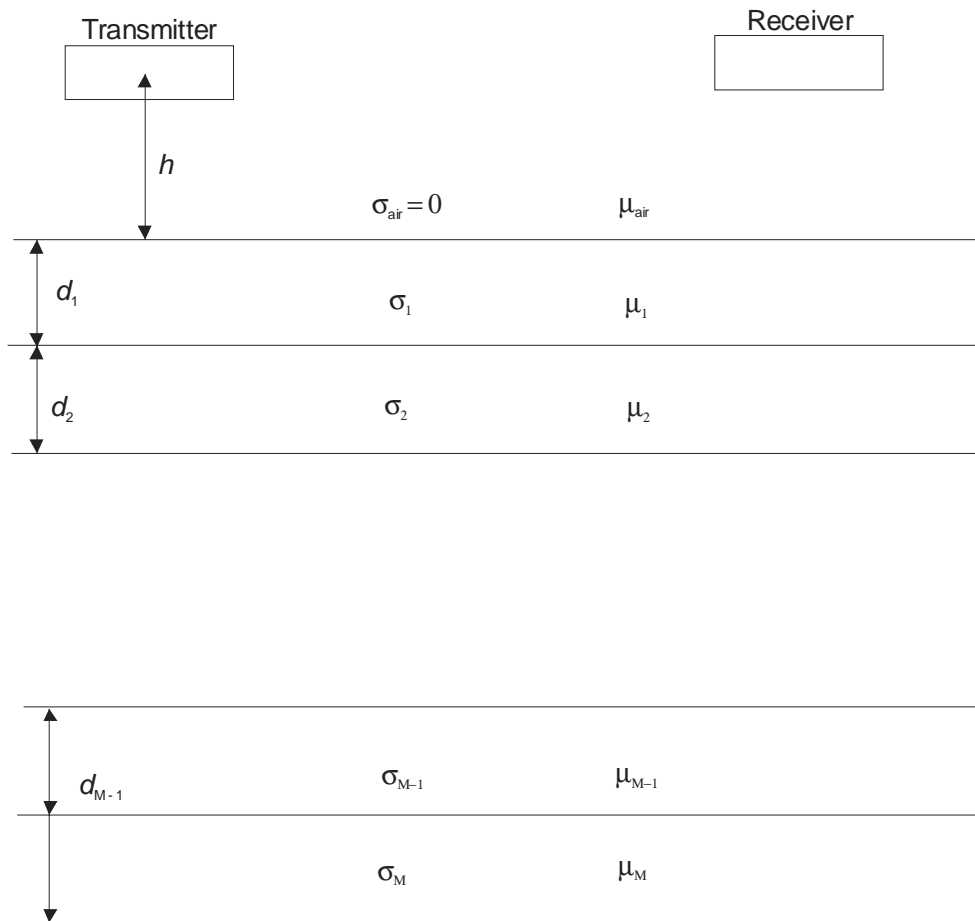


Figure 2. Schematic of the model for layered soil conductivity profiles. d is the thickness of the soil layer, σ is the apparent electrical conductivity, μ is the magnetic permeability, h is the height, and M is the number of layers.

$$Y_{M-1} = N_{M-1} \frac{N_M + N_{M-1} \tanh(u_{M-1} d_{M-1})}{N_{M-1} + N_M \tanh(u_{M-1} d_{M-1})} \quad [24]$$

where

$$u_k = \sqrt{\lambda^2 + i\sigma_{ak}\mu_k\omega} \quad [25]$$

The apparent conductivity measurements $m^V(h)$ (vertical mode) and $m^H(h)$ (horizontal mode) at height h above the ground could be predicted by using the input of apparent electrical conductivity of k^{th} layer (σ_{ak}) which was incorporated in T_0 and T_2 :

$$m^V(h) = (4\mu_0\omega r^2) \text{Im}(1 + B^3 T_0) \quad [26]$$

$$m^H(h) = (4\mu_0\omega r^2) \text{Im}(1 + B^2 T_2) \quad [27]$$

where

$$T_0 = -\int_0^\infty R_0(gB/r) g^2 e^{-2gh/\delta} J_0(gB) dg \quad [28]$$

$$T_2 = -\int_0^\infty R_0(gB/r) g e^{-2gh/\delta} J_1(gB) dg \quad [29]$$

$J_i(\)$ is the Bessel function of the first kind in which i is the order number (Zwillinger, 1996), r is the intercoil space, δ is the scaling factor ($=\sqrt{2/\sigma_1\mu_0\omega}$) where δ_1 is the apparent conductivity of layer 1, B is another scaling factor ($=r/\delta$), and $R_0(\lambda)$ is:

$$R_0(\lambda) = \frac{N_0 - Y_1}{N_0 + Y_1} \quad [30]$$

Temperature effect: Before a comparison can be made between the modeled apparent soil electrical conductivity and the one measured in the field with the EM38 ground conductivity meter, both conductivities have to be at the same reference temperature of 25°C. The modeled apparent electrical conductivities were already at this reference since the Rhoades model and Eqs. [17]–[19] assumed a temperature of 25°C. The electrical conductivities measured in the field were converted using the following equation:

$$\sigma_{25^{\circ}\text{C}} = f_T \sigma_T \quad [31]$$

where $\sigma_{25^{\circ}\text{C}}$ is the electrical conductivity at 25°C, σ_T is the electrical conductivity at temperature T (°C), and f_T is a temperature conversion factor.

The temperature conversion factor used in this study was one taken from Sheets and Hendrickx (1995):

$$f_T = 0.4470 + 1.4034 e^{-T/26.815} \quad [32]$$

Based on the climate data from the New Mexico Climate Center, during 1999 the annual average air temperature was 15°C. The maximum and minimum soil temperatures at 7.5 cm depth were 30 and 0°C, respectively.

Soil temperature at specific depths and times were obtained by equations from Carslaw et al. (1959) with the assumption that the soil surface temperature fluctuation was the same as the soil temperature fluctuation at depth 7.5 cm:

$$T(z,t) = T_A + A \exp(z/d) \sin(\omega t + z/d) \quad -\infty < z < 0 \quad [33]$$

where

$$d = \sqrt{2K_T / \omega} = \sqrt{K_T \tau / \pi} \quad [34]$$

T is the temperature (K), T_A is the annual average temperature, A is the amplitude of the surface temperature fluctuation (K), z is the soil depth (L), d is the damping depth (L), ω is the angular frequency (T^{-1}), t is the time (T), τ is the period of the wave (T), and K_T is the thermal diffusivity (L^2/T).

Since EM38 provides a maximum depth of exploration of 150 cm in vertical dipole mode I calculated daily soil temperatures from Eqs. [33]–[34] for depths of 0, 25, 50, 75, 100, 125, and 150 cm during January 1999. The mean soil temperature at depth 0–150 cm during January turned out 5.7°C (Figure 3). The temperature 5.7°C (= T) was presumed to be used for the electrical conductivity at temperature in the field. To overcome temperature effects on EM38 readings, those readings (σ_T) were corrected to the reference temperature of 25°C by multiplying by 1.58 (= f_T).

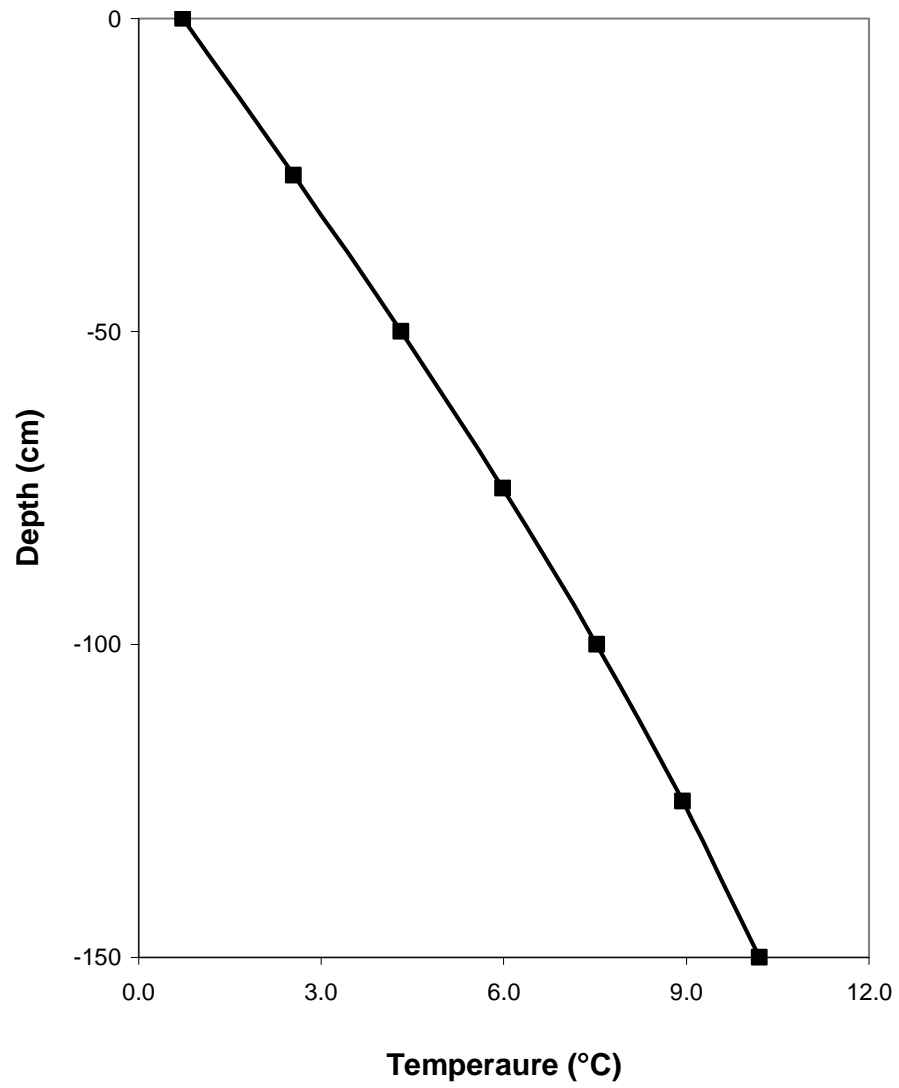


Figure 3. Mean soil temperature profile during January 1999, calculated using Eqs. [33]–[34].

3. RESULTS AND DISCUSSION

3.1 Characterization of the Representative Soil Profiles

Table 4 presents the field characteristics of the six representative soil profiles. There were distinct differences between the Cottonwood and Saltcedar sites. The mean ground water table depths were 159 and 225 cm for, respectively, the Cottonwood and Saltcedar sites. Yet, in spite of the shallower ground water table in the Cottonwood sites their mean ground water quality was 397 ppm which was considerably better than the 1703 ppm measured in the Saltcedar sites. The mean amplitudes of the ground water table fluctuations were 47 and 27 cm for, respectively, the Cottonwood and Saltcedar sites. The relatively short mean distance to the river of 127 m for the Cottonwood sites versus 423 m for the Saltcedar explains the larger ground water fluctuations at the Cottonwood sites. The closer distance to the river resulted in a much quicker and stronger response of ground water tables to changes in river water levels. Finally, the mean apparent electrical conductivity or soil salinity of the Cottonwood sites was 40 mS/m and much lower than the 212 mS/m measured at the Saltcedar sites. The value of 40 mS/m is below the threshold value of approximately 50–60 mS/m above which Cottonwood survival and productivity are seriously impaired (Sheets et al., 1994).

Table 4. Field characteristics of the six representative soil profiles.

Profile	Vegetation	Mean GWT ¹	Mean GWFA ²	GWQ ³	Distance from river	EM38 ⁴ (mS/m)				n ⁵
						max	min	mean	median	
1	Cottonwood	155	61	240	70 m	72	1	23	28	8
2	Cottonwood	176	47	280	170 m	88	7	42	50	7
3	Cottonwood	145	32	670	140 m	151	22	76	80	10
4	Saltcedar	231	26	1190	450 m	260	30	171	149	7
5	Saltcedar	224	18	1950	420 m	430	42	261	315	6
6	Saltcedar	221	36	1970	400 m	442	75	313	333	9

¹Ground water table depth from the soil surface (cm)

²Ground water fluctuation amplitude (cm)

³Current ground water quality (TDS) (July, 1999)

⁴EM38 reading in vertical mode with penetration depth 1.5 m

⁵Number of readings

The spatial variability of field-measured apparent electrical conductivities was quite large (Hendrickx et al., 1992, 1994; Sheets et al., 1994) and my research area was no exception. Table 4 shows a wide range of values around the mean apparent electrical conductivity as measured in a radius of approximately 30 m around each of the representative profile. Yet, in spite of this large variability the ranking from low to high salinity was consistent for the mean, maximum, minimum, and median values which made my six soil profiles representative for riparian soil conditions in the Middle Rio Grande Valley.

Table 5 presents the texture and soil hydraulic properties for each soil horizon of the six profiles in the form of Van Genuchten parameters. The three soil profiles at the Cottonwood site had a coarser texture than those at the Saltcedar site. Also, the Cottonwood site soils were more homogeneous than those at the Saltcedar site. Since it was not possible to take undisturbed core samples in all horizons, I determined soil texture for some of the horizons in the field to derive Van Genuchten parameters. When the soil textural class was obtained by tactile analysis (i.e., “by feel”) in the field, the Carsel et al. (1988) Van Genuchten parameters were used. In horizons with laboratory measurements of the percentages of sand, clay, and silt the neural networks of Schaap et al. (1996) were used to derive the Van Genuchten parameters.

I made root observations in the soil pits and derived root distributions for Cottonwood and Saltcedar (Figure 4). These root distributions were quite similar to those observed by Moayyad (2001) in the Bosque del Apache in New Mexico located about 150 km south of my sites. The root density was highest in the top 50 cm of the soil profile and diminished with depth. Below 220 cm no more roots were observed.

Table 5. Soil stratigraphy and Van Genuchten model parameters for the six representative soil profiles.

Profile	Soil depth (cm)	Texture [§]	θ_r	θ_s	α (cm ⁻¹)	n (-)	K_{sat} (cm/d)
1	0-8	SIL [#]	0.072	0.39	0.027	1.29	12
	8-28	SL*	0.055	0.31	0.034	3.71	131
	28-92	S [†]	0.045	0.43	0.145	2.68	713
	>92	CS*	0.047	0.34	0.039	3.74	2348
2	0-5	L [†]	0.078	0.43	0.036	1.56	25
	5-15	LS [†]	0.057	0.41	0.124	2.28	350
	15-60	LS*	0.050	0.43	0.015	3.84	226
	60-132	S [†]	0.045	0.43	0.145	2.68	713
	132-165	S*	0.049	0.41	0.023	4.74	1125
	>165	CS*	0.047	0.34	0.039	3.74	2348
3	0-20	L [†]	0.078	0.43	0.036	1.56	25
	20-130	S [†]	0.045	0.43	0.145	2.28	713
	>130	CS*	0.047	0.34	0.039	3.74	2348
4	0-10	SC [†]	0.100	0.38	0.027	1.23	3
	10-51	C [#]	0.096	0.48	0.017	1.27	17
	51-81	CL [#]	0.085	0.45	0.011	1.43	11
	81-185	SL [#]	0.036	0.39	0.043	1.56	77
	185-260	S [†]	0.045	0.43	0.145	2.68	713
	>260	CS*	0.047	0.34	0.039	3.74	2348
5	0-12	C*	0.051	0.42	0.006	2.57	0.4
	12-19	L [†]	0.078	0.43	0.036	1.56	25
	19-27	SCL [†]	0.100	0.39	0.059	1.48	31
	27-35	C*	0.051	0.42	0.006	2.57	0.4
	35-88	L [†]	0.078	0.43	0.036	1.56	25
	88-225	SCL [†]	0.100	0.39	0.059	1.48	31
	225-285	LS*	0.047	0.34	0.015	3.54	160
	>285	CS*	0.047	0.34	0.039	3.74	2348
6	0-38	C*	0.051	0.42	0.006	2.57	0.4
	38-79	C*	0.062	0.44	0.003	1.85	0.02
	79-109	SC*	0.053	0.47	0.004	1.56	3
	109-236	SI [#]	0.085	0.46	0.008	1.51	12
	236-290	LS*	0.047	0.34	0.015	3.54	160
	>290	CS*	0.047	0.34	0.039	3.74	2348

[§]SIL: Silt loam, SL: Sandy loam, S: Sand, L: Loam, LS: Loamy sand, SC: Sandy clay, C: Clay, CL: Clay loam, SCL: Sandy clay loam, SI: Silt, CS: Coarse sand

*Measured in Hendrickx's soil physics laboratory

[#]Neural networks (Schaap et al., 1996)

[†]Carsel et al. (1988)

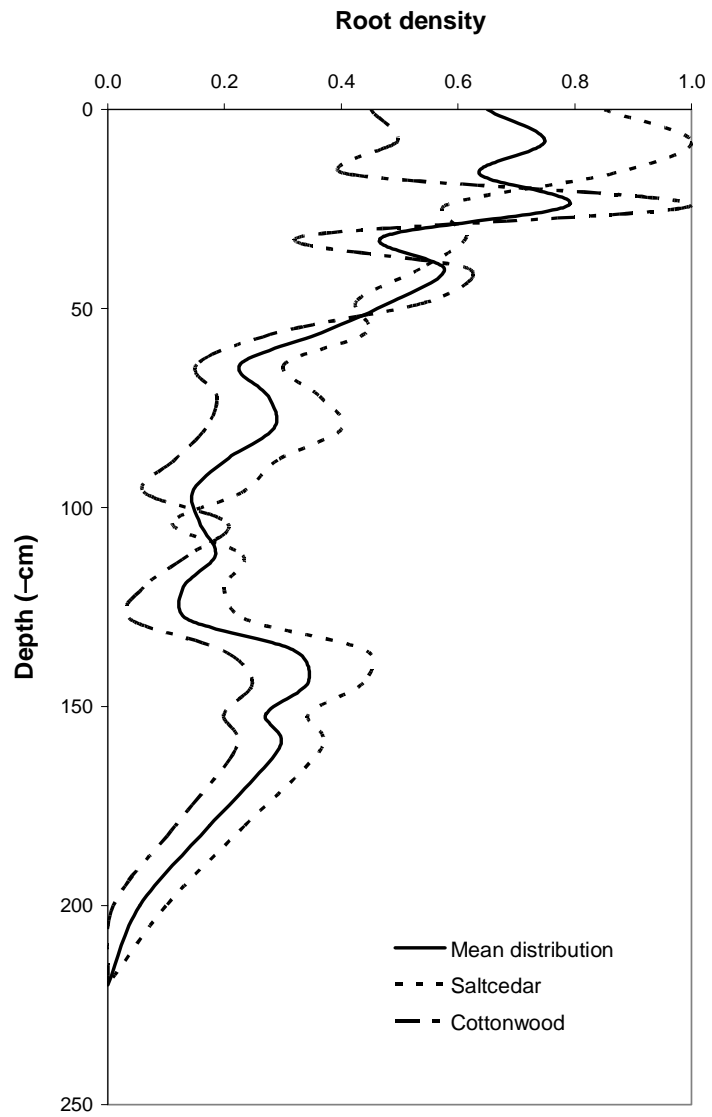


Figure 4. Root density distribution of the Saltcedar and Cottonwood (maximum density = 1).

The Feddes' root model uptake parameters in this study were taken from the work by Moayyad (2001), since he matched the Feddes' parameters to correlate the actual evapotranspiration in the Bosque del Apache. This study adapted his Feddes' parameters from the non-flooded area vegetation to adjust the evapotranspiration. Since the root distributions of Cottonwood and Saltcedar were so similar in my sites, I used the same root distribution and Feddes' parameters (Table 6) for both vegetation types for all simulations. This approach eliminated the effect of root distribution differences on my simulations.

3.2 Soil Salinity Modeling in Representative Profiles

The water content, soil-salt content, and soil-water concentration profiles after 30 years in the 5 m model domain depth are presented in Figure 5–7. The total amount of the salt and the mean soil-water concentration in the rootzone over 60 years are plotted in Figure 8 to examine the soil salinity development over time. The initial ground water and the time-independent bottom solute boundary conditions were 200 ppm in all six profiles, to observe the effect of soil texture and ground water dynamics on soil salinity.

Cottonwood profiles (Profiles 1–3) accumulated a smaller amount of salt in the rootzone than Saltcedar profiles (Profiles 4–6). Profiles 1–3 had coarser soil texture, shallower ground water table, and larger ground water fluctuation. Since ground water fluctuation moved through the layer of maximum salt contents (Figures 5–6) the salts were “washed out” by the ground water and the rootzone remains at low salinity levels. On the other hand, higher soil salinity occurred in Profiles 4–6 because the finer soil's

Table 6. Model Feddes' root uptake parameters.

Parameter	Value
P0 ¹	-0.1 cm
P0pt ²	-2 cm
P2H ³	-80 cm
P2L ⁴	-250 cm
P3 ⁵	-1500 cm
r2H	0.75 cm/day
r2L	0.5 cm/day

¹Soil-water pressure below which root uptake starts

²Soil-water pressure below which root uptake water is at the maximum rate

³Soil-water pressure below which root uptake is limited by both potential transpiration rate and the r2H.

⁴Soil-water pressure below which root uptake is limited by both the potential transpiration rate and the r2L.

⁵Soil-water pressure below which root uptake stops

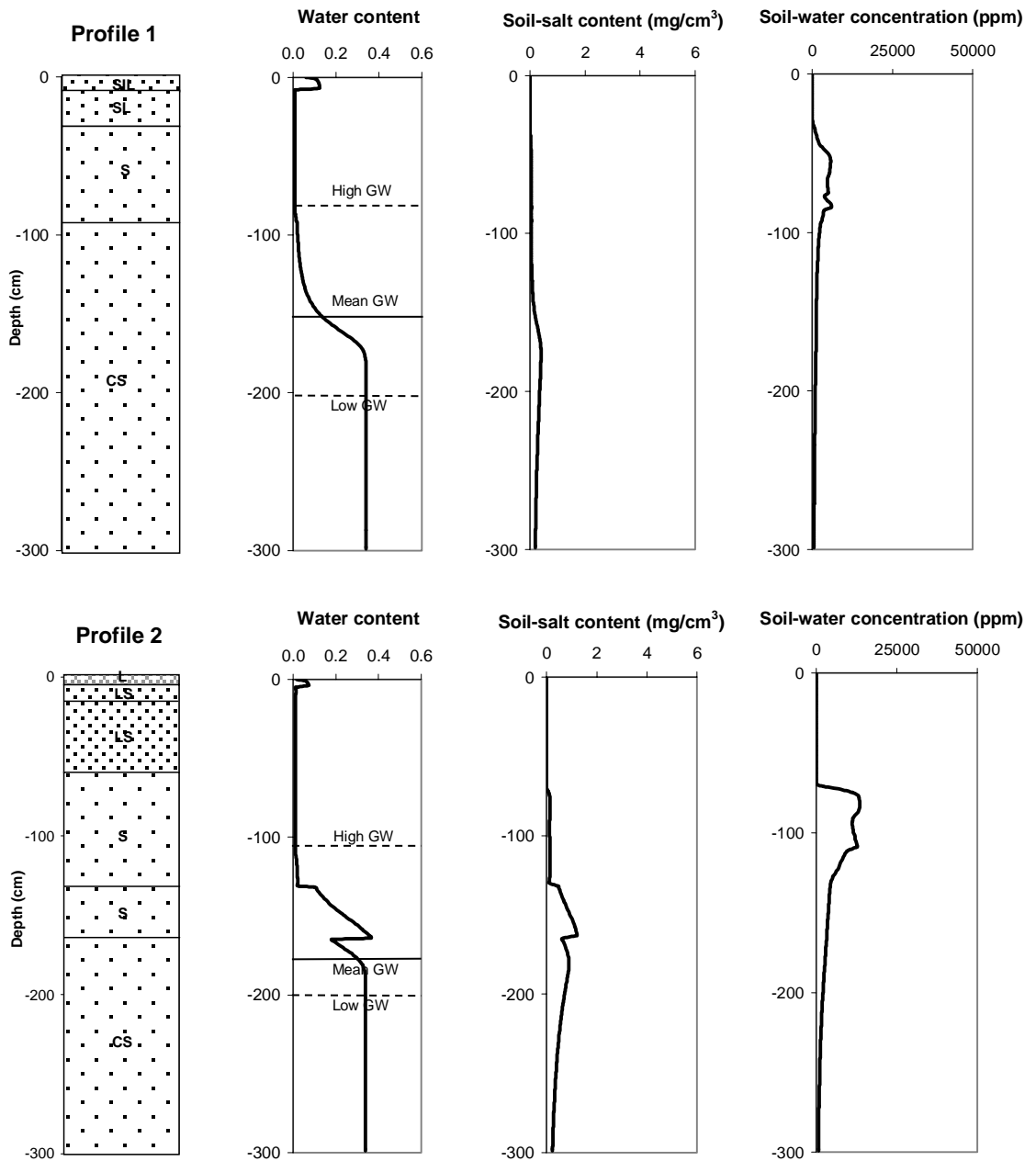


Figure 5. Soil stratigraphy and texture of representative profiles 1 and 2 with the profile of the water content, soil-salt content, and soil-water concentration after 30 years in the 5 m model domain depth and ground water table depth (mean, high, and low). Initial ground water and time-independent bottom solute boundary conditions are 200 ppm (SIL: silty loam, SL: sandy loam, S: sand, L: loam, LS: loamy sand, CS: coarse sand).

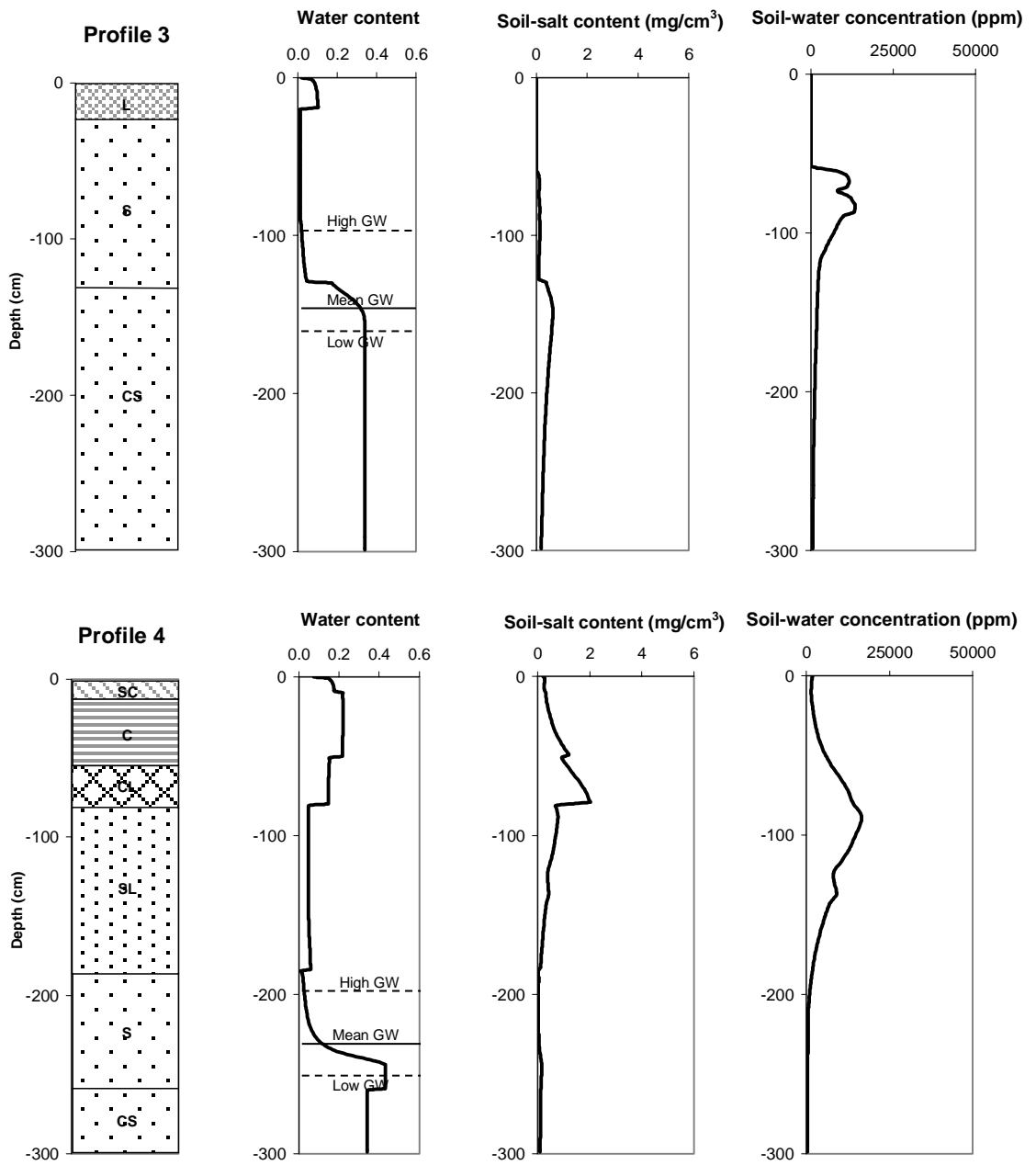


Figure 6. Soil stratigraphy and texture of representative profiles 3 and 4 with the profile of the water content, soil-salt content, and soil-water concentration after 30 years in the 5 m model domain depth and ground water table depth (mean, high, and low). Initial ground water and time-independent bottom solute boundary conditions are 200 ppm (SC: sandy clay, C: clay, CL: clay loam).

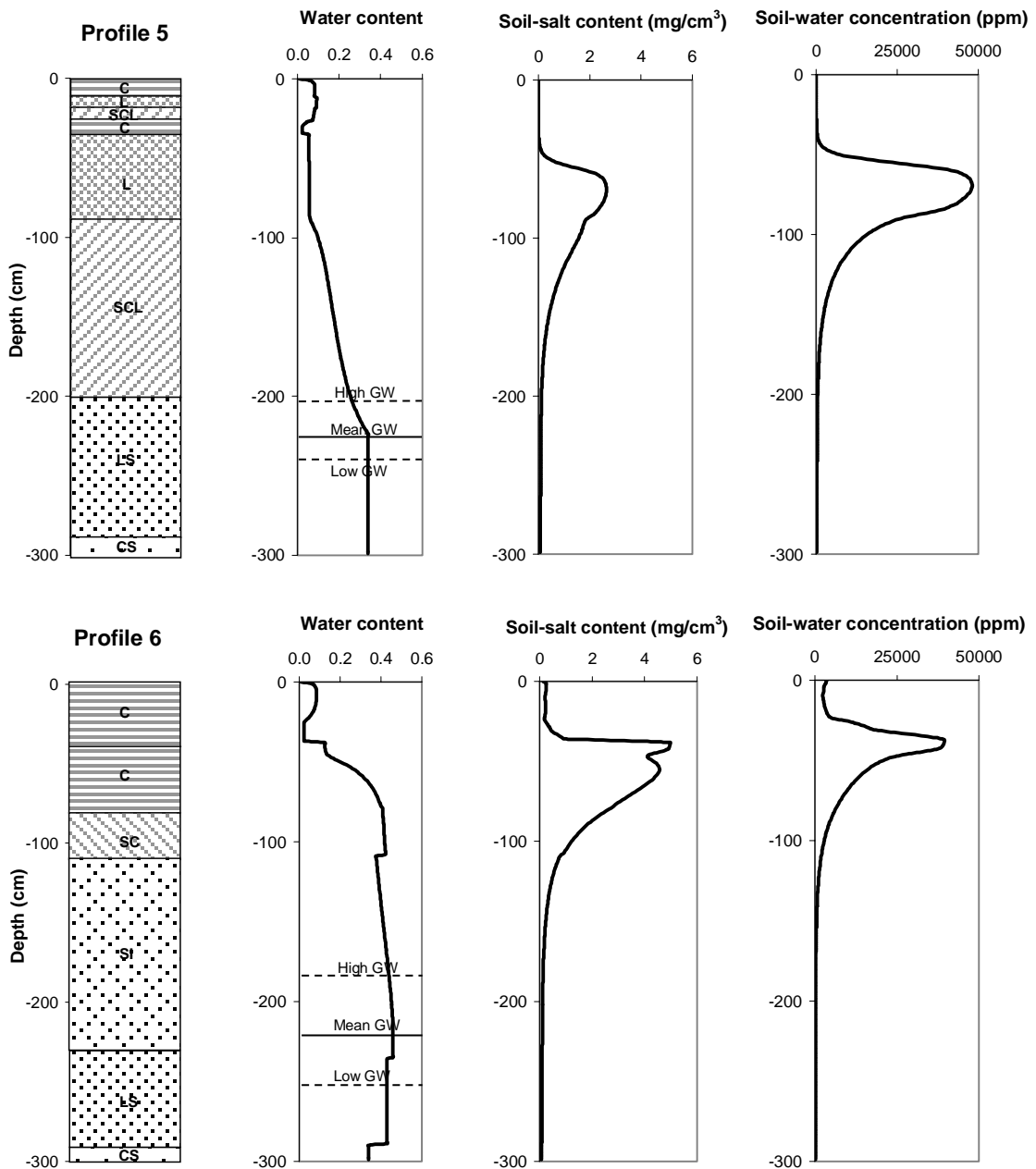


Figure 7. Soil stratigraphy and texture of representative profiles 5 and 6 with the profile of the water content, soil-salt content, and soil-water concentration after 30 years in the 5 m model domain depth and ground water table depth (mean, high, and low). Initial ground water and time-independent bottom solute boundary conditions are 200 ppm (SCL: sandy clay loam, SI: silt).

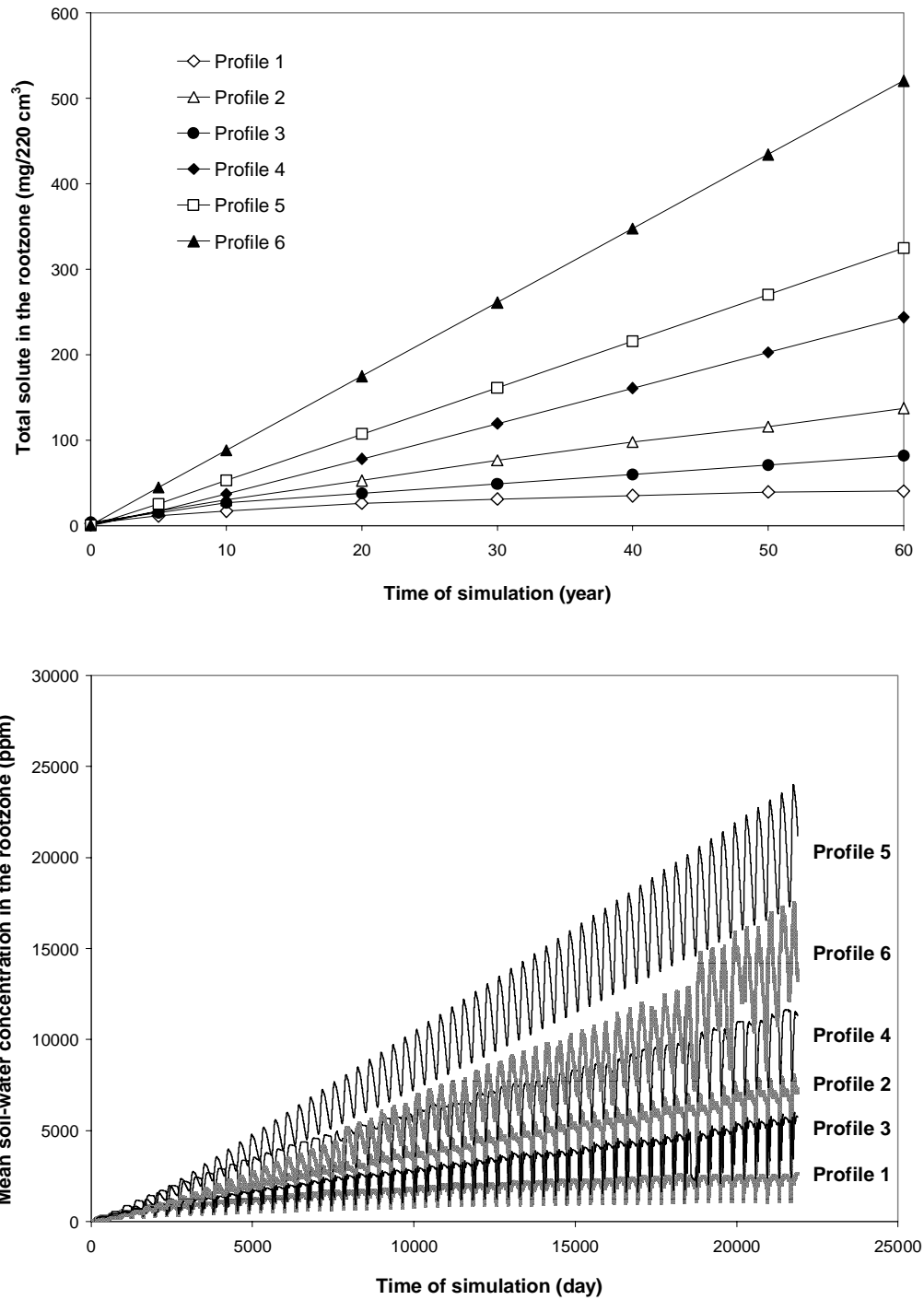


Figure 8. Total amount of the salt (Top) and mean soil-water concentration (Bottom) in the rootzone over time (initial ground water and time-independent bottom solute boundary conditions are 200 ppm, 5 m model domain depth).

large capillary fluxes brought salt close to the soil surface out of reach for the ground water (Figure 6–7). Therefore, these profiles accumulated large amounts of salt in the rootzone.

In Figure 8 bottom, the combination of the ground water table depth and the amount of evapotranspiration affected the seasonal soil salinity variation. However, the overall rootzone soil salinity in Profile 1 reached a sustainable steady state after about 20 years. Compared to Profile 1, Profiles 2–3 had smaller ground water fluctuations and finer soil texture which caused a slow but gradual increase in soil salinity over time. In Profiles 4–6, soil salinity increased rapidly over time because of the height of capillary rise of the fine-textured soil and deeper ground water table depth. These results indicated that soil texture as well as ground water table depth and its fluctuation played an important role in soil salinity in arid riparian areas.

Figures 9 and 10 present the simulated soil salinity profiles for both the 5- and 20-m-deep model domains after 30 and 60 years of simulations. These profiles were obtained using the measured TDS for ground water at the six profiles. The initial condition of all six profiles was a soil without salts.

The simulated soil salinity increased gradually from very low in Profile 1 to high in Profile 6. It was striking how well the simulated soil salinity profiles agreed with the measured salinity ranking presented in Table 4; the increasing mean apparent electrical conductivity measured with the EM38 ground conductivity meter coincided with an increasing maximum concentration simulated in the six profiles.

In Profiles 5 and 6, the simulated salt concentrations at depths 50–100 cm obtained values of about 290,000 to 1,000,000 ppm. Salt concentrations exceeding

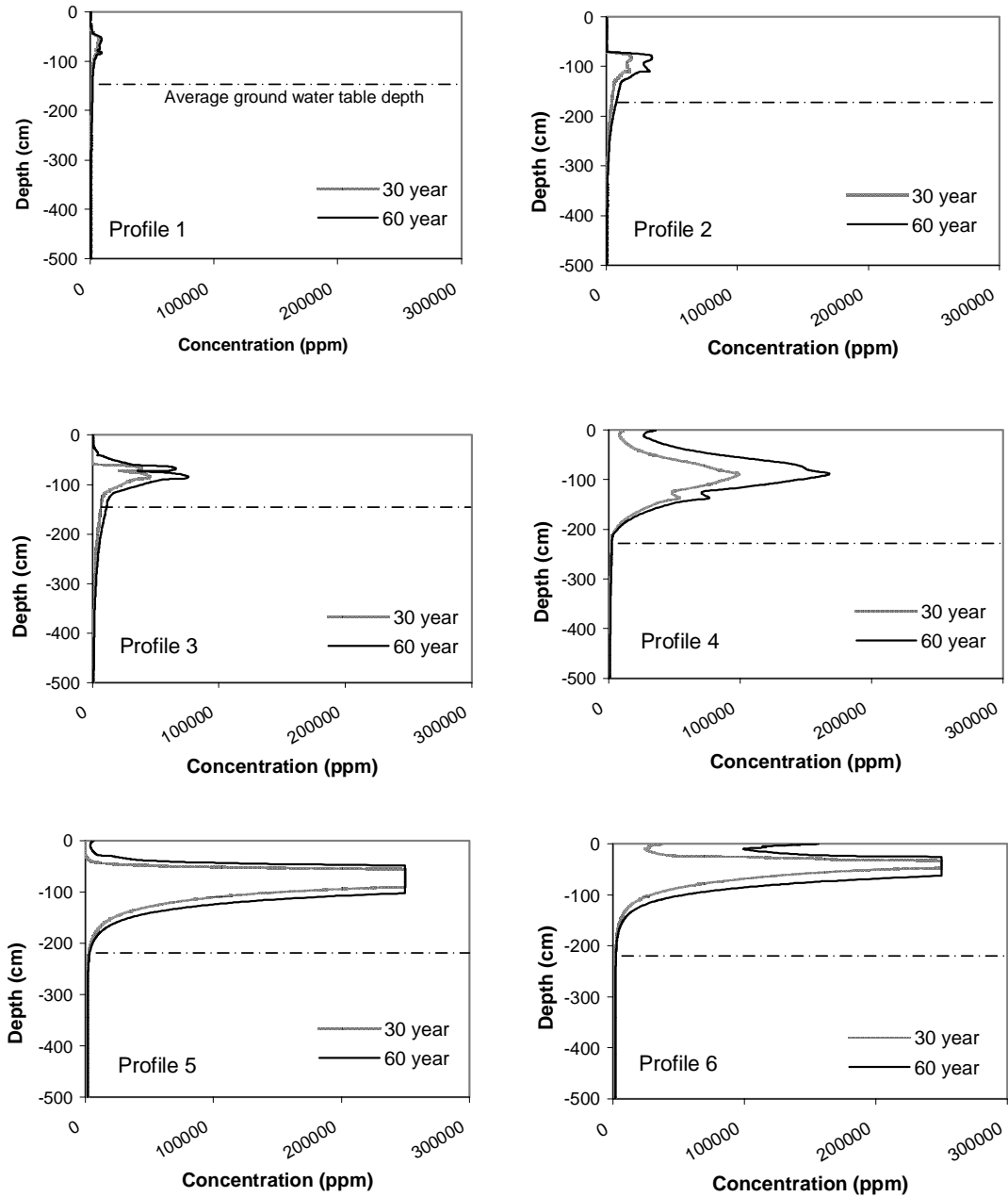


Figure 9. The soil-water solute concentration profiles after 30 and 60 years in the 5 m model domain depth (Profiles 1–3: Cottonwood; Profiles 4–6: Saltcedar).

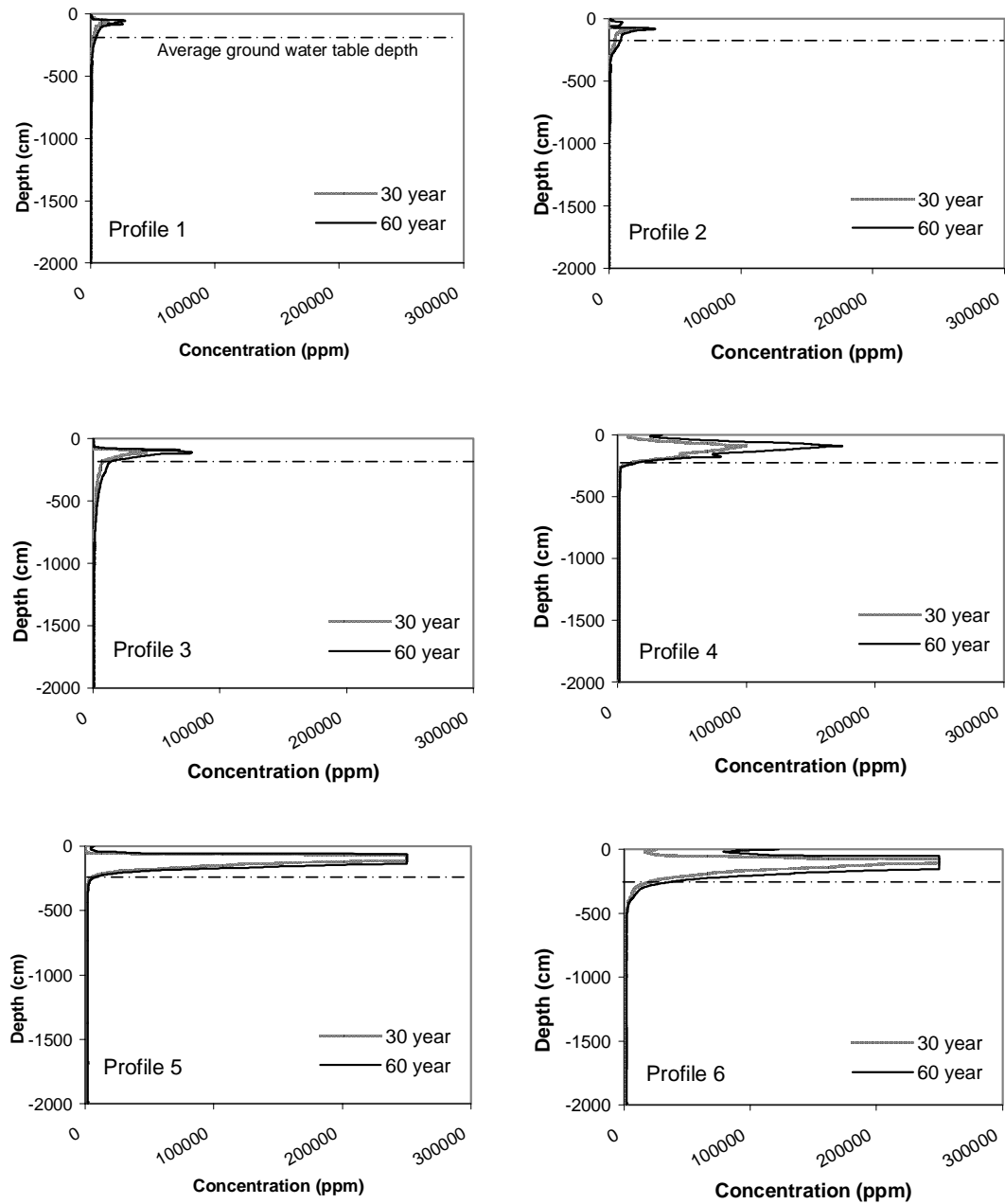


Figure 10. The soil-water solute concentration profiles after 30 and 60 years in the 20 m model domain depth (Profiles 1–3: Cottonwood; Profiles 4–6: Saltcedar).

250,000 ppm were a correct representation of the total salt mass accumulated at a given depth but not of the true concentration in the soil solution since the NaCl solubility in water at 25°C is 250,000 ppm. The physical meaning of a salt concentration higher than 250,000 ppm is a soil volume with a soil solution concentration of 250,000 ppm and the remainder of the salts deposited in solid form. Therefore, I have taken 250,000 ppm as the maximum salt concentration possible in the soil solution in Figures 9 and 10. Also for the calculation of the apparent soil electrical conductivity 250,000 ppm was the maximum concentration employed. However, in the HYDRUS-1D simulations I allowed the salt concentrations to increase without limitation in order to preserve a good salt mass balance.

The development of soil salinity over time differed widely from profile to profile. In Profile 1 soil salinity hardly increased over time whereas in Profiles 4 through 6 soil salinity doubled between year 30 and 60. Also in Profiles 2 and 3, soil salinity was increasing over time but at a much slower rate. The soil hydrological characteristics of Profiles 1–3 were ideal for salt-sensitive Cottonwood while those in Profiles 4–6 resulted in soil salinization and invasion of salt-tolerant Saltcedars.

The depth profiles of soil solution concentrations (Figures 9 and 10) simulated with HYDRUS-1D have been transformed in depth profiles of apparent soil electrical conductivities using Eqs. [17]–[19] and Procedure I of Rhoades et al. (1990) at a reference temperature of 25°C. Next, the nonlinear model for prediction of a vertical EM38 ground conductivity meter reading (Eqs. [20]–[30]) was used to obtain a predicted EM38 measurement at each of the six profiles. This prediction was corrected for the soil temperature at the time of the EM38 measurements in the field using Eqs. [31]–[32].

Figures 11 and 12 compare the field-measured values of the apparent electrical soil conductivity for each of the six profiles (Table 4) with those predicted by the HYDRUS-1D model and Eqs. [17]–[30] using current TDS values of the ground water as well as TDS values of 200, 500, 1000, and 2000 ppm.

Using current TDS values the predictions of the apparent soil profile electrical conductivity for Profiles 1 through 3 all fell within the ranges of the field-measured values while those for Profiles 4 through 6 always overestimated these ranges. One plausible explanation for this is that ground water quality at the latter profiles has been considerably better in the past than at the present. Until about 30 years ago before the construction of Cochiti Reservoir, flooding was a common occurrence in the riparian areas around Albuquerque and must have resulted in lower TDS values in the shallow ground water. Indeed, the simulations using ground water TDS values of 200 and 500 ppm resulted in predicted values that fell well within the range of field-measured values.

The good agreement between predicted and measured EM38 values demonstrate that simulations with HYDRUS-1D yield soil salinity predictions that concur well with those measured in the field.

3.3 Sensitivity Analysis

Table 7 shows the results of the sensitivity analysis in terms of the total amount of soluble salts accumulated in the 220 cm rootzone during 30 and 60 years of simulation assuming a ground water quality of 2000 ppm and as the normalized total amount of soluble salts. The latter is the more important number since it reflects the propensity of a

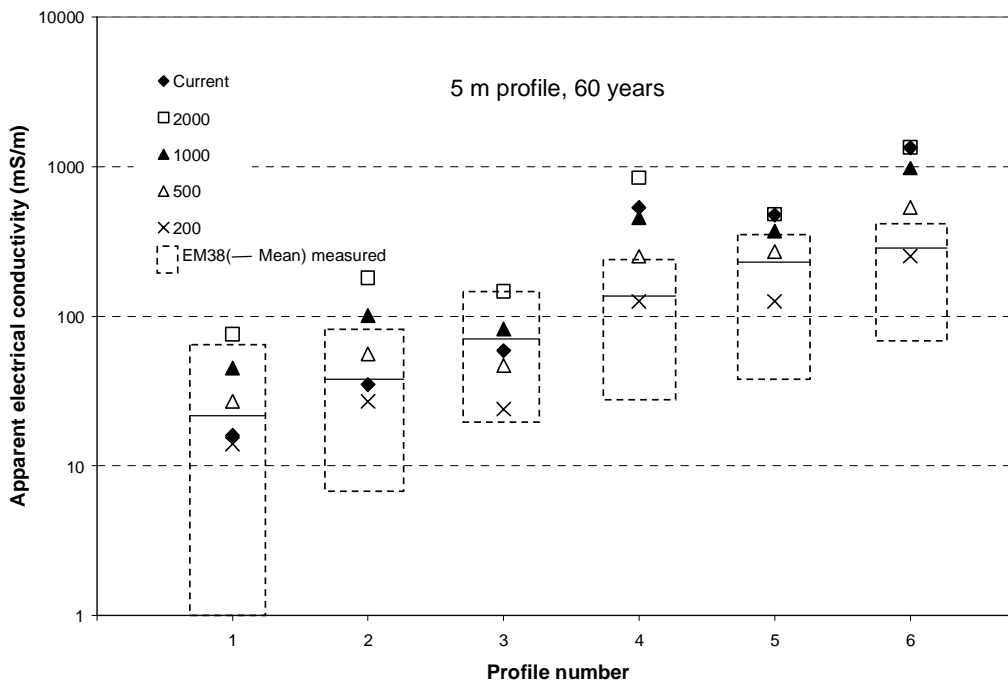
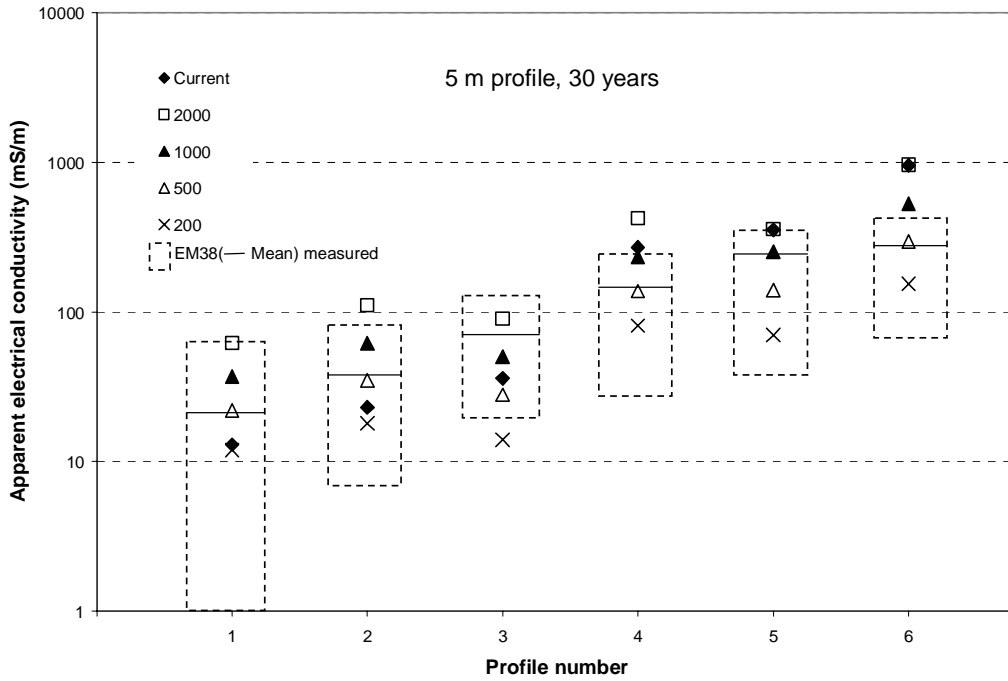


Figure 11. Comparison between modeled and measured apparent electrical conductivity of soil in 5 m soil profile (dotted square shows the range of EM38 field measurement).

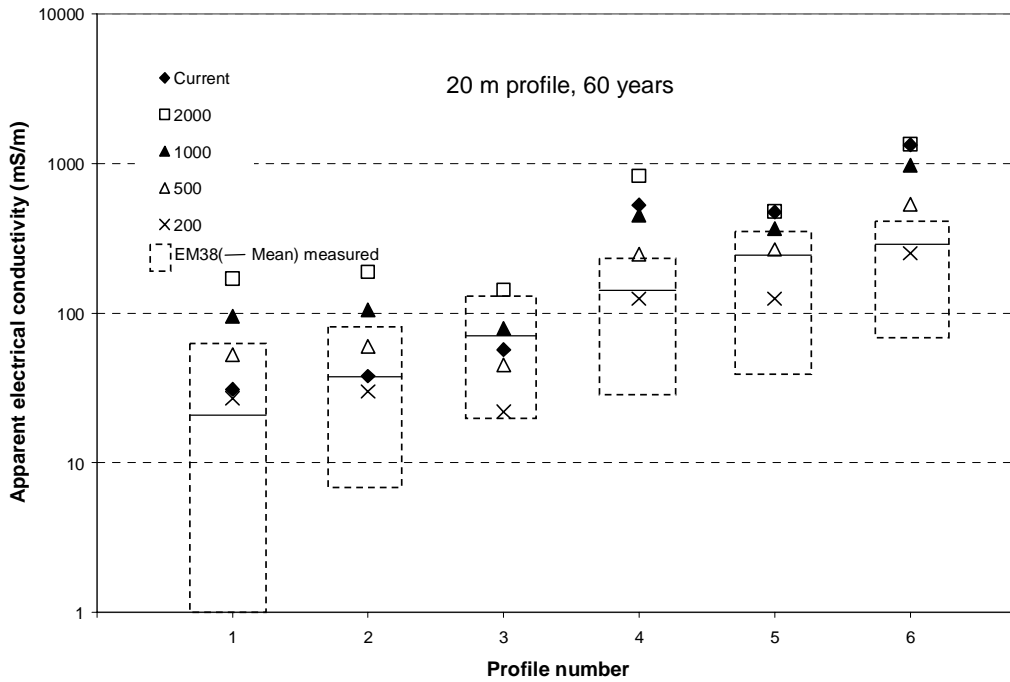
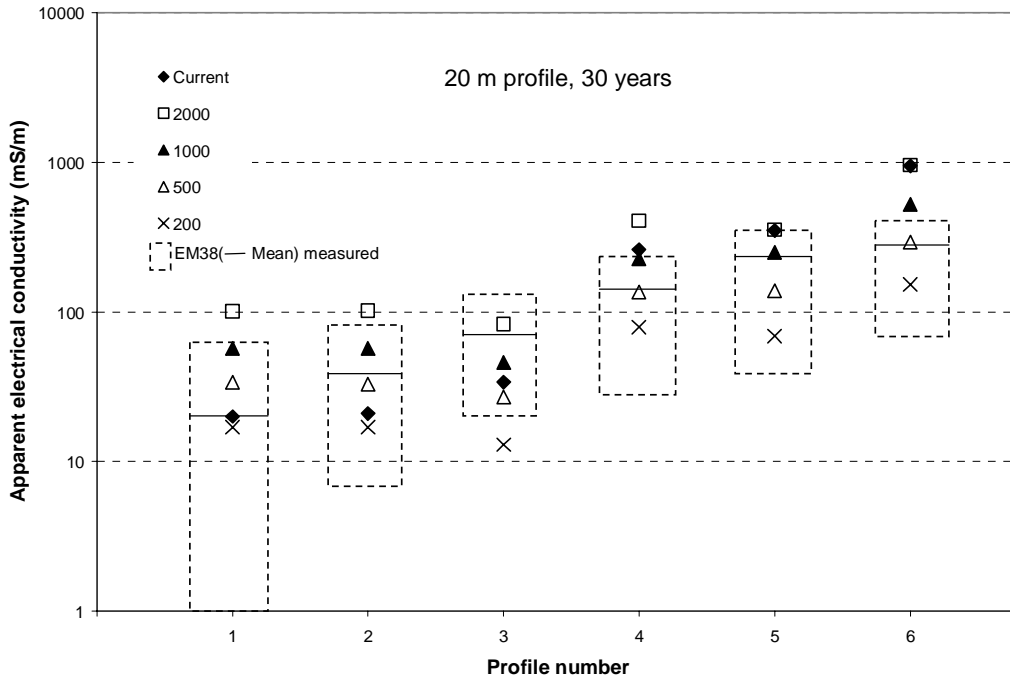


Figure 12. Comparison between modeled and measured apparent electrical conductivity of soil in 20 m soil profile.

Table 7. Results of the sensitivity analysis, showing the outcome of each scenario in terms of the total amount of soluble salts in the rootzone (220 cm).

Scenario	Normalized total amount of soluble salts in the rootzone	Total amount of soluble salts in the rootzone (g/220cm ³)
1	0.99	24.7
2	0.99	24.5
3	0.49	12.3
4	0.49	12.2
5	1.00	24.8
6	1.00	24.9
7	0.50	12.4
8	0.50	12.4
9	0.93	23.3
10	0.92	23.0
11	0.46	11.5
12	0.46	11.4
13	0.71	17.6
14	0.69	17.3
15	0.35	8.7
16	0.34	8.6
17	0.04	1.0
18	0.02	0.6
19	0.02	0.5
20	0.02	0.4
21	0.06	1.5
22	0.06	1.4
23	0.03	0.8
24	0.03	0.8
25	0.01	0.2
26	0.00	0.1
27	0.01	0.1
28	0.00	0.1
29	0.00	0.0
30	0.00	0.0
31	0.00	0.0
32	0.00	0.0

soil profile for soil salinization. For example, scenarios 29–32 have a low risk for soil salinization while scenarios 1–2 and 5–6 have a high risk.

Table 8 presents the sensitivity (Eq. [10]) and relative effects of each factor considered in the sensitivity analysis. Soil texture which determines the amount of capillary rise is by far the most important factor for soil salinity in the riparian area that I have investigated. The next factor is time with a relative impact of 0.35: in most cases the longer a soil profile was exposed to conditions leading to soil salinization the higher the soil salinity will become (Figure 8–10). The third factor is the depth to the ground water table which had a relative impact of 0.13 while the amplitude of ground water fluctuations and the depth of the model domain had a negligible impact.

The importance of soil texture has been corroborated by a study in the Bosque del Apache near Socorro, New Mexico, where it was found that soil texture/stratigraphy as derived from a geomorphological interpretation of 1935 aerial photos of the Rio Grande had a strong relationship with current soil salinity levels (Personal Communication, 2001, Drs. Harrison and Borchers).

The effects of ground water depth, fluctuation, and aquifer flux—the latter was represented by the two domain depths—were small compared to the effects of soil texture and time in my study area which was typical for many riparian areas in the Middle Rio Grande Valley. Thus, the risk for soil salinization could be predicted quite well from only soil profile information where mean ground water levels varied from 200 to 300 cm with fluctuations of 100 cm around the mean or less. This was an important finding since soil texture did not change with time and could always be evaluated in the field during the planning of riparian restoration projects.

Table 8. Main effects of soil texture, average ground water depth, ground water fluctuation amplitude, time of simulation, and depth model domain factors on the total amount of the soluble salts in the rootzone (220 cm) TSS_{root} .

Factor	Effect on TSS_{root}	
	g/220 cm ³	Relative Effect
<i><u>Main Effects</u></i>		
Soil Texture	16.4	1.00
Average Ground Water Depth	2.1	0.13
Ground Water Fluctuation Amplitude	0.9	0.06
Time of Simulation	5.8	0.35
Depth Model Domain	0.1	0.01

3.4 Soil Salinity in Arid Riparian Areas in the Middle Rio Grande Valley

The purpose of this section is to discuss in greater detail the factors that affect soil salinity in arid riparian areas in the Middle Rio Grande Valley using the results of the previous two sections. I will focus the discussion on the six representative soil profiles.

The main factor determining soil salinity is *soil texture*: Profiles 1–3 with the coarsest soil texture were much lower saline than Profiles 4–6 with a finer soil texture (Table 4). The loamy sand became much lower saline than the loam in the sensitivity analysis. The reason for this is that a coarser soil texture generally resulted in hydraulic soil properties that allowed much lower capillary rise to occur than a fine soil texture. The great difference in capillary rise between loamy sand and loam is demonstrated in Table 2.

The differences in capillary flux between the six representative soil profiles are demonstrated in Table 9. Capillary fluxes in all profiles reduced when the ground water table depth increased from 100 to 300 cm. At a ground water table depth of 100 cm without vegetation Profiles 1–3 had no capillary flux at all while the finer textured Profiles 4–6 had capillary fluxes from 0.04 to 0.14 cm/day. Profile 6 contained a high percentage of clay with small pores that allowed a high capillary rise but with a limited flux due to the low hydraulic conductivity of the clay. This explains the low capillary flux of clay Profile 6 versus the higher fluxes in Profiles 4 and 5. In contrast, at a ground water table depth of 300 cm the small pores of the clay made a capillary flux of 0.02 cm/day possible while the larger pores of Profiles 4 and 5 could not sustain any capillary flux at all. Since Profile 6 maintained a capillary rise at all ground water table depths it

Table 9. Capillary fluxes entering the rootzone from the ground water table for the six representative profiles at three constant ground water levels and with three rootzone thicknesses. Roots have uniform distribution throughout the rootzone.

Profile	Capillary Flux (cm/day)		
	GWT ¹ = 100 cm	200 cm	300 cm
Rootzone = 0; No vegetation			
1	0.00	0.00	0.00
2	0.00	0.00	0.00
3	0.00	0.00	0.00
4	0.14	0.00	0.00
5	0.11	0.00	0.00
6	0.04	0.04	0.02
Rootzone = 100 cm			
1	0.00	0.00	0.00
2	0.00	0.00	0.00
3	0.14	0.00	0.00
4	1.00	0.14	0.00
5	0.11	0.00	0.00
6	0.04	0.04	0.02
Rootzone = 200 cm			
1	0.00	0.00	0.00
2	0.00	0.00	0.00
3	0.14	0.22	0.00
4	0.72	0.43	0.00
5	0.11	0.00	0.00
6	0.04	0.04	0.02

¹Constant ground water table depth from the soil surface

became the most saline profile of the six representative soil profiles under the field conditions at my research sites. Had ground water levels never dropped below 100 cm, Profiles 4 and 5 would have become the most saline profiles.

Vegetation generally increased the amount of capillary rise lost to the atmosphere. The deeper the rootzone, the less height of capillary rise in the soil was needed to bring the water where roots could suck it up for transpiration. For example, in Profile 4 the capillary flux at ground water table depth 100 cm without vegetation was 0.14 cm/day while with rootzones of 100 and 200 cm the capillary fluxes became, respectively, 1.00 and 0.72 cm/day.

Overall, the trends shown in Table 9 agree quite well with the simulated salt accumulation in the profiles (Table 10) as well as the field measured soil salinity (Table 4). However, I could not simply compare the ranks of capillary fluxes in Table 9 with the ranks of salt accumulation in Table 10 since capillary rise is a complex phenomenon with many interactions between soil texture, soil profile layering, ground water table depth (Hendrickx et al., 2002) and vegetation. The zero capillary fluxes in Profiles 1 and 2 explained the lowest salt accumulations in these profiles. The low capillary flux of Profile 6 led to the highest salt accumulation because this profile could transport salts all the time even during periods of deep ground water tables. The higher salt accumulation in Profile 4 than in Profile 3 could be understood from Table 9 but the large amount of salt accumulation in Profile 5 could not have been predicted from Table 9. Thus, this table shows clearly the principles involved but misses some aspects of soil salinization. To completely capture the dynamics of soil salinization a model like HYDRUS-2D has to be used. Indeed, the rankings in Table 10 and Table 4 coincide for all six profiles which is

Table 10. Total amount of soluble salts [g / (220 or 500 cm³)] accumulated in the representative profiles after simulations using current ground water TDS values.

Profile	5 m profile				20 m profile			
	30 year		60 year		30 year		60 year	
	0-2.2m	0-5m	0-2.2m	0-5m	0-2.2m	0-5m	0-2.2m	0-5m
1	0.04	0.09	0.05	0.11	0.07	0.15	0.13	0.27
2	0.11	0.18	0.19	0.31	0.10	0.17	0.18	0.32
3	0.18	0.33	0.30	0.52	0.16	0.32	0.29	0.55
4	0.71	0.85	1.46	1.61	0.69	0.83	1.45	1.60
5	1.57	1.77	3.17	3.37	1.57	1.76	3.16	3.36
6	2.56	2.76	5.09	5.29	2.55	2.74	5.09	5.28

another validation of HYDRUS-1D.

The field observations of soil profile layering, the EM38 measurements, the analysis of capillary fluxes in homogeneous and heterogeneous soil profiles, the salinity profiles predicted by HYDRUS-1D, and the EM38 values predicted through Eqs. [17]–[30] demonstrated that *soil texture* is the most important soil factor for salinization in my research area due to its impact on capillary fluxes from the ground water table.

Time is the next important factor determining soil salinity. If some salts accumulate every year in the profile, the final soil salinity will become high even if ground water quality is good. For example, Table 11 shows the amount of salts accumulated in the six representative profiles assuming a ground water quality of 200 ppm during the 60 years of simulation. In spite of the high quality ground water, salinization occurred even in the least sensitive Profile 1. All rootzones saw an increase in salinization from 0 to 30 years and from 30 to 60 years. It is expected that problems with soil salinity in non-flooded riparian areas of the Middle Rio Grande Valley will increase rather than decrease over the coming decades.

This study demonstrated how ground water table monitoring, measurements of soil hydraulic properties, and simulations with the model HYDRUS-1D allowed water managers to predict the future development of soil salinity. Those predictions can be used to determine land use or to decide on soil restoration measures.

It was somewhat a surprise that ground water dynamics had such a minor impact in the sensitivity study. One reason for surprise is that in my study area ground water levels were relatively deep—from about 200 to 300 cm. Yet, a closer look at the soil salinity depth profiles (Figures 5–7 and 9–10) and total amount of salt accumulation in

Table 11. Total amount of soluble salts [g / (220 or 500 cm³)] in the representative profiles after simulations with 200 ppm ground water quality.

Profile	5 m profile				20 m profile			
	30 year		60 year		30 year		60 year	
	0–2.2m	0–5m	0–2.2m	0–5m	0–2.2m	0–5m	0–2.2m	0–5m
1	0.03	0.08	0.04	0.09	0.06	0.12	0.11	0.22
2	0.08	0.13	0.14	0.22	0.07	0.12	0.13	0.23
3	0.05	0.10	0.09	0.15	0.05	0.10	0.09	0.17
4	0.12	0.14	0.25	0.27	0.12	0.14	0.24	0.27
5	0.16	0.18	0.33	0.35	0.16	0.18	0.32	0.34
6	0.26	0.28	0.52	0.54	0.26	0.28	0.52	0.54

the 220 cm rootzone and 500 cm soil profile (Tables 10 and 11) revealed much about the impact of ground water table dynamics on soil salinity.

Be reminded that the 20-m-deep simulation profile represents a situation with a stagnant aquifer through which no salts were being removed. The depth of 20 m was chosen on the basis of preliminary simulations which showed that no major salt concentrations reached 20 m depth during the 60 years of simulation. The 5-m-deep simulation profile was set up in such a way that water leaving the domain at 5 m depth contained the salt content present at the bottom of the domain, but water entering the domain by capillary rise contained a salt content equal to the current TDS level at each of the six profiles in Table 10 and 200 ppm in Table 11. As explained in the Methods and Materials section this was a crude way to simulate salt removal by horizontal flow in an aquifer. The salt accumulations in the 5- and 20-m-deep simulation domains in Tables 10 and 11 were almost identical except for Profile 1. For example, in Profile 6 in the 5-m-deep profile the 0–5-m-deep soil layer contained $0.54 \text{ g}/500 \text{ cm}^3$ after 60 years which was identical to the $0.54 \text{ g}/500 \text{ cm}^3$ found in the 20-m-deep simulation domain. On the other hand, in Profile 1 the amount of salt in the 5-m-deep domain was $0.09 \text{ g}/500 \text{ cm}^3$ which was less than half the $0.22 \text{ g}/500 \text{ cm}^3$ found in the 20-m-deep domain. This is evidence that a large amount of salt has been “removed” by the shallow aquifer underlying the 5-m-deep soil layer. The same effect but greatly reduced could be seen when comparing the salt amount in the 0–5-m-deep soil layer after 60 years in Profiles 2 and 3. No such effect at all was found in the more saline Saltcedar Profiles 4–6.

To understand why these differences occurred I inspected the salt amounts in the rootzone (0–2.2 m) versus those in the top 5 m of the soil profile. In Profiles 1–3 in both

the 5- and 20-m-deep simulation domains the salt amount stored in the rootzone was about half of the amount stored in the top 5 m. This means that about half of the salt was stored between depths 2.2–5.0 m where it was prone to flushing by the flux in the shallow aquifer since the mean ground water table depth was considerably less than 2.2 m (Table 4). In Profiles 4–6 almost all the salt was stored in the 2.2-m-deep rootzone well above the mean average ground water table depth in these profiles (Table 4). Due to the large capillary fluxes that carried the water and the salts into the rootzone, the salts accumulated at such shallow depths in the soil profile that they could not be reached by the fluctuating ground water table. They will remain in the soil profile forever unless the river changes course and floods these high salinity profiles. This was a regular event before the canalization of the Rio Grande but after implementation of flood control measures floods have become very rare events. As a result soil salinity keeps increasing in vulnerable areas unless soil restoration is implemented.

Figures 5–7 and 9–10 also clearly demonstrate that in Profiles 1–3 the salts concentrated within reach of the ground water table while in Profiles 4–6 the salts accumulated above the ground water table. Therefore, I hypothesize that a coupled vadose zone/ground water system that allowed salt removal through flow in the aquifer, even if the ground water table was shallow, would result in a lower soil salinity in Profiles 1–3. It might even lead to a stable system of low salt profiles over time. On the other hand, such a modeling effort would not change the basic dynamics of increasing soil salinity with time in Profiles 4–6 since the ground water table could not reach the accumulated salts.

Tables 10–11 and Figures 5–10 clearly demonstrate that ground water dynamics

kept some riparian areas salt free. The dynamics worked best where the soil texture only permitted a small amount of capillary rise so that the salts accumulated close to the water table. Where the soil texture of the soil profile was such that large capillary fluxes were moving water and salt high into the profile out of reach for the ground water, soil salinity will occur and become more severe over time (Figure 8).

To investigate the surface infiltration effect on soil salinity I have modeled salt concentrations for different infiltration scenarios. The soil salinity profiles after a prolonged period without any infiltration events and 40 days later are presented in Figure 13. As expected the soil salinity distribution has not changed much. To demonstrate that deep infiltration after extremely wet periods played only a minor role, I have plotted in Figure 14 the soil salinity depth profiles after the wettest season (200 days) and after the major infiltration event (20 days) in my simulations. Although some rain water infiltrated deep into the profile, it did not affect the salt distribution much. This is the another proof that salt-free soil profiles in the riparian areas of the Middle Rio Grande Valley were caused by ground water dynamics.

3.5. Effect of Evapotranspiration on Soil Salinity

In order to determine the validity of my conclusions concerning the soil salinization process I also need to explore how well my simulations predicted the evapotranspiration of riparian vegetation and the effect of cumulative evapotranspiration on soil salinization. The correct prediction of evapotranspiration of riparian vegetation was possible with HYDRUS-1D as has been shown by Moayyad (2001). However, many input data were needed: meteorological data, hydraulic properties of soil profile, root

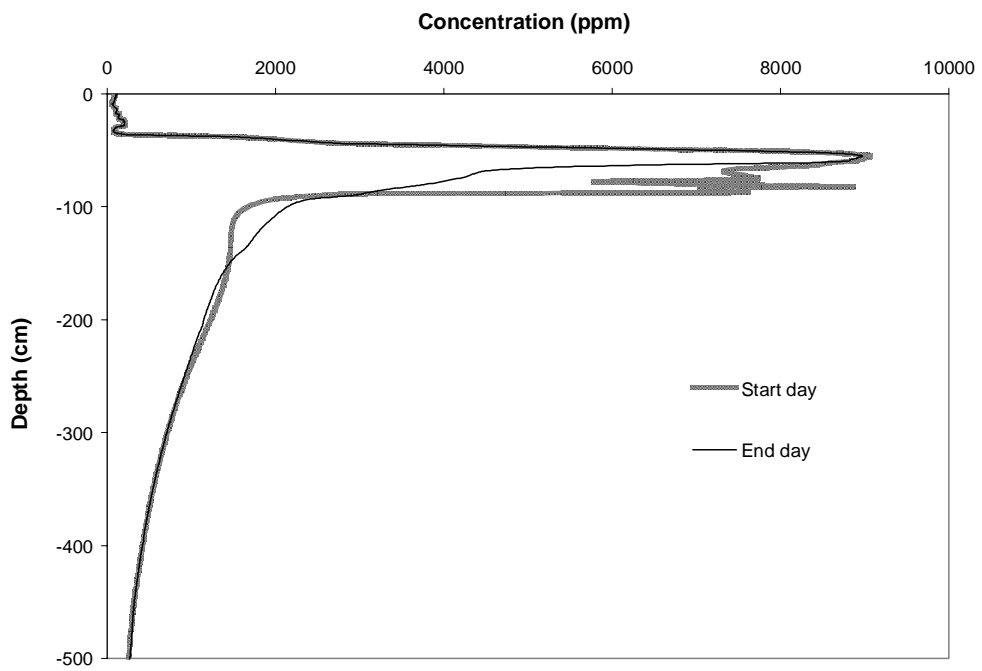


Figure 13. Salt distribution profiles during period without infiltration events in Profile 1 (start: 17280 day, end: 17320 day).

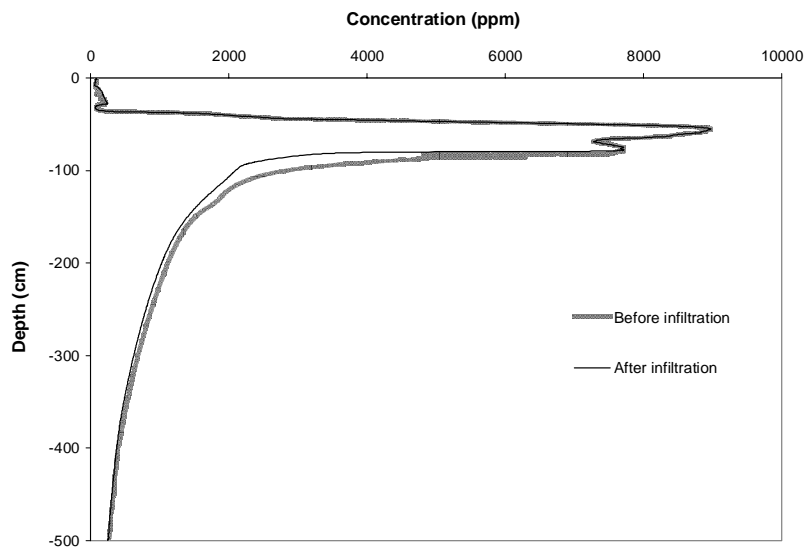
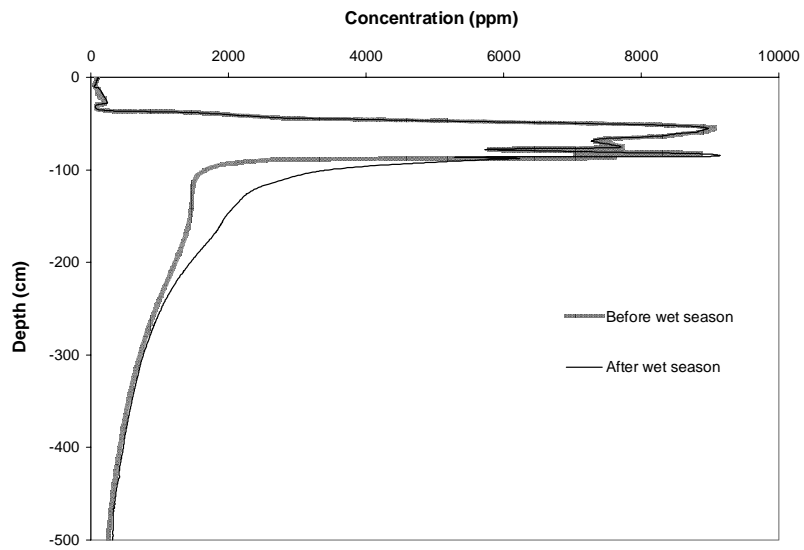


Figure 14. Salt distribution profiles during the wettest season (top) and during the major infiltration event (bottom) in Profile 1.

distribution, root water uptake function, and depth of ground water table.

First, I calculated in Table 12 for the month of September the crop coefficients of Cottonwood and Saltcedar using the actual evapotranspiration simulated with HYDRUS-1D and the measured potential evapotranspiration at the Rio Grande Nursery weather station. I have selected the month of September for the calculations of the crop coefficients since an independent estimate of the evapotranspiration for Cottonwood was available for September 14, 2000, from remote sensing data. No estimate for the Saltcedar was available since the Saltcedar in my research area already had been removed in preparation for restoration.

The average crop coefficients for the Cottonwoods and Saltcedars in the month of September were, respectively, 0.30 and 0.38. These crop coefficients appeared lower than the ones measured in other areas of the Albuquerque and Socorro Bosques (Personal communication, 2002, Drs. Cleverly and Bawazir). One reason might be that the soil hydrology at my six soil profiles was such that the evapotranspiration was indeed lower.

To check this I compared the crop coefficients of Cottonwood measured from remote sensing data on September 14, 2000, using the Surface Energy Balance Algorithm for Land (SEBAL) (Bastiaanssen et al., 1998a, b) for Cottonwoods with the ones resulting from my simulations. Although the HYDRUS-1D and SEBAL derived crop coefficients for Profiles 2 and 3 were quite different, the mean crop coefficient 0.37 estimated by SEBAL was in reasonable agreement with the one derived from my HYDRUS-1D simulations.

Another reason for my lower values might be the way I have simulated root water uptake. My measured root distribution functions (see Figure 4) might not reflect

Table 12. Comparison between modeled and SEBAL evapotranspiration and crop coefficient.

Profile	HYDRUS (Septembers 1995–1999)					SEBAL (September 14 2000)		
	Root distribution					PET [%] (mm/d)	ET (mm/d)	Kc (-)
	PET* (mm/d)	Observed		Uniform				
ET [#] (mm/d)		Kc ⁺ (-)	ET (mm/d)	Kc (-)				
1	5.32	1.58	0.30	1.90	0.36	6.85	2.26	0.33
2	5.32	1.75	0.33	1.85	0.35	6.79	1.29	0.19
3	5.32	1.38	0.26	1.55	0.29	6.95	4.10	0.59
4	5.32	1.49	0.28	1.65	0.31	-	-	-
5	5.32	1.94	0.36	2.51	0.47	-	-	-
6	5.32	2.73	0.51	3.82	0.72	-	-	-

*Potential evapotranspiration obtained from weather data at the Rio Grande Nursery weather station in Albuquerque

Actual evapotranspiration

+ Crop coefficient (actual ET / potential ET)

% Potential evapotranspiration calculated from SEBAL algorithm

what phreatophytes really do, i.e., take up water where it is available in the soil profile. For this reason I have repeated all my simulations with a uniform root distribution over the entire depth of the soil profile. Such a root distribution led to a higher evapotranspiration as is shown in Table 12. The mean daily evapotranspiration of the Cottonwood and Saltcedar increased, respectively, from 1.6 to 1.8 mm and from 2.1 to 2.7 mm. The crop coefficients for September also increased. The mean crop coefficients for Cottonwood and Saltcedar increased to, respectively, 0.33 and 0.5.

For this thesis it was of interest to explore how the higher ET affects soil salinization. Figure 15 presents the soil salinity profiles for the simulations with the observed and the uniform root distributions. Although the uniform root distributions clearly led to a higher soil salinity due to a higher total evapotranspiration, the basic characteristics of soil salinity have not been changed. The salt accumulation occurred at the same depth in the profile. Thus, although a higher ET resulted in a rate of soil salinization, it did not affect the basic processes of soil salinization and the removal of salts by ground water fluctuations in the coarse soils with Cottonwoods. Figure 15 also shows how much soil salinization processes depend on soil hydraulic properties. The change in root distribution hardly led to higher predicted EM38 observations.

The data presented in Figures 13–15 and in Table 12 clearly show that the principal factor for soil salinization is the composition of the soil profile. Evapotranspiration affected the degree of soil salinity over time, but did not affect the basic processes of salt removal and accumulation.

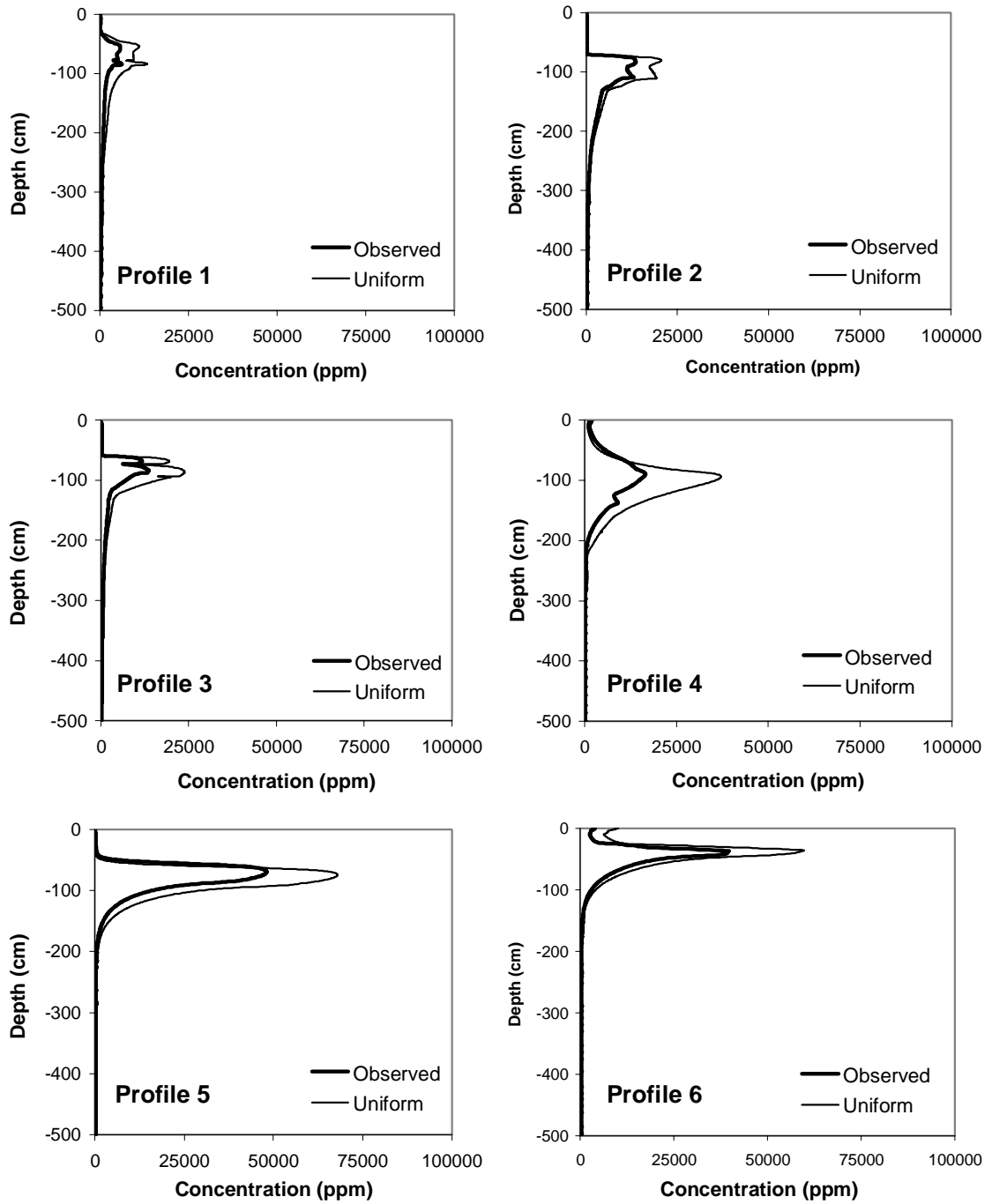


Figure 15. Solute concentration profiles using observed and uniform root distribution after 30 years in the model depth (bottom solute boundary condition: 200 ppm).

4. CONCLUSIONS

The objectives of this study were to validate the model HYDRUS-1D for prediction of long-term soil salinity in arid non-flooded riparian areas of the Middle Rio Grande Valley and to determine the key factors causing riparian soil salinity in order to answer the question whether a small amount of deep infiltration or ground water table dynamics keeps some riparian rootzones salt free. The following conclusions can be drawn from my study:

1. Soil salinization is a complex process, influenced by a number of hydrogeologic factors such as hydraulic properties of soils, ground water table fluctuation, ground water quality, aquifer flux, and time. The results of the sensitivity analysis show that soil texture is the most important factor for soil salinity in my riparian study area since it determines the amount of capillary rise.
2. The sand soils in my study area did not become salinized over long periods of time. The low height of capillary rise in these soils resulted in salts accumulation close to the water table where salts are washed out by ground water fluctuations. The salinization of clay soils increased with time because the large capillary rise of the fine-textured soil caused salt accumulation near the soil surface out of reach

for washing by the ground water.

3. Some rain water infiltrates deeper into the profile after storm events, but excess infiltration plays no role in decreasing the salt concentration in my riparian study area.
4. Evapotranspiration affects the degree of soil salinity over time, but does not affect the basic processes of salt removal and accumulation.
5. The good agreement between predicted and measured EM38 values proves that HYDRUS-1D is a useful simulation tool to evaluate soil salinity in arid riparian areas.

REFERENCES

- Bastiaanssen, W.G.M., M. Menenti, R.A. Feddes, and A.A.M. Holtslag. 1998a. A remote sensing surface energy balance algorithm for land (SEBAL). 1. Formulation. *J. Hydrol.* 212-213:198-212.
- Bastiaanssen, W.G.M., H. Pelgrum, J. Wang, Y. Ma, J.F. Moreno, G.J. Roerink, and T. van der Wal. 1998b. A remote sensing surface energy balance algorithm for land (SEBAL). 2. Validation. *J. Hydrol.* 212-213:213-229
- Brady, N.C., and R.R. Weil. 1999. *The nature and properties of soils*. 12th ed. Prentice Hall. New Jersey.
- Carslaw, H.S., and J.C. Jaeger. 1959. *Conduction of heat in soils*. Oxford University Press. London.
- Carsel R.F., and R.S. Parrish. 1988. Developing joint probability distributions of soil water retention characteristics. *Water Resour. Res.* 24:755-769.
- Childs, S.W., and R.J. Hanks. 1975. Model of soil salinity effects on crop growth. *Soil Sci. Soc. Am. Proc.* 39:617-622.
- Feddes, R.A., P.J. Kowalik, and H. Zaradny. 1978. *Simulation of field water use and crop yield*. John Wiley & Sons, New York, New York.
- Hanson, B., S.R. Grattan, and A. Fulton. 1993. *Agricultural salinity and drainage*. Univ. of Cal. Irrig. Program Handbook Publ. No. 3375. Univ. of Cal., Davis.
- Hendrickx, J.M.H. 1990. Determination of hydraulic soil properties. p. 43-92. *In* M.G. Anderson and T.P. Burt (ed.) *Process studies in hillslope hydrology*. John Wiley & Sons, New York, New York.
- Hendrickx, J.M.H., B. Baerends, Z.I. Raza, M. Sadiq, and M.A. Chaudhry. 1992. Soil salinity assessment by electromagnetic induction on irrigated land. *Soil Sci. Soc. Am. J.* 56:1933-1941.

- Hendrickx, J.M.H., C.D. Grande, B.A. Buchanan, and R.E. Bretz. 1994. Electromagnetic induction for restoration of saline environments in New Mexico. p. 247-265. *In* R.K. Bhada, A. Ghassemi, T.J. Ward, M. Jamshidi, and M. Shahinpoor (ed.) ECM Series on Environmental Management & Intelligent Manufacturing. No. 1 “Waste-management: From Risk to Remediation” ECM Press, Albuquerque, New Mexico.
- Hendrickx, J.M.H., J. Beekman, R. Koch, and G. Rodriguez. 1997. Salinity survey for revegetation potential along the Rio Grande in the Paso Del Norte region. A report to the El Paso Field Division of the U.S. Bureau of Reclamation.
- Hendrickx, J.M.H., B. Borchers, D.L. Corwin, S.M. Lesch, AC. Hilgendorf, and J. Schlue. 2002. Inversion of soil conductivity profiles from electromagnetic Induction measurements: Theory and experimental verification. *Soil Sci. Soc. Am. J.* 66:673-685.
- Hussain, G., and O.J. Helweg. 1994. Effect of saline irrigation water on tree growth. *J. Irrig. and Drain. Eng.* 120: 970-978.
- Huyakorn, P.S., J.B. Kool, and J.B. Robertson. 1989. VAM2D–Variably saturated analysis model in two dimensions. Version 5.0 with hysteresis and chained decay transport. Documentation and user’s guide. NUREG/CR-5352 HGL/89-01, Hydrogeologic, 8, Int. Assoc. of Hydrogeologist, Heise, Germany.
- Kruse, E.G., D.F. Champion, D.L. Cuevas, R.E. Yoder, and D. Young. 1993. Crop water use from shallow, saline water table. *Trans. Am. Soc. Agric. Eng.* 36:697-707.
- Law, A.M., and D.M. Kelton. 1999. Simulation modeling and analysis. 3rd ed. McGraw-Hill. New York.
- Leij, F.J., and M.Th. Van Genuchten. 2000. Solute transport. p. A:183-227. *In* M.E. Sumner (ed.) Handbook of soil science. CRC Press, Boca Raton, Florida.
- Marthaler, H.P., W. Vogelsanger, F. Richard, and P.J. Wierenga. 1983. A pressure transducer for field tensiometers. *Soil Sci. Soc. Am. J.* 47:624-627.
- Moayyad, B. 2001. Importance of ground water depth, soil texture, and rooting depth on arid riparian evapotranspiration. M.S. Independent Study, Hydrology Program, New Mexico Tech.
- Popp, C.J., C.M. Jensen, D.K. Brandvold, and L.A. Brandvold. 1982. Precipitation Analysis in Central New Mexico. p. 2:89-101. *In* L.H. Keith (ed.) Energy and Environmental Chemistry Acid Rain. Ann Arbor Science.

- Prathaper, S.A., C.W. Robbins, W.S. Meyer, and N.S. Jayawardance. 1992. Models for estimation capillary rise in a heavy clay soil with a saline shallow water table. *Irrig. Sci.* 13:1-7.
- Rhoades, J.D., N.A. Manteghi, P.J. Shouse, and W.J. Alves. 1989. Soil electrical conductivity and soil salinity: New formulations and calibrations. *Soil Sci. Soc. Am. J.* 53:433-439.
- Rhoades, J.D., P.J. Shouse, W.J. Alves, N.A. Manteghi, and S.M. Lesch. 1990. Determining soil salinity from soil electrical conductivity using different models. *Soil Sci. Soc. Am. J.* 54:46-54.
- Schaap, M.G., and W. Bouten. 1996. Modeling water retention curves of sandy soils using neural networks. *Water Resour. Res.* 32:3033-3040.
- Sheets, K.R., J.P. Taylor, and J.M.H. Hendrickx. 1994. Rapid salinity mapping by electromagnetic induction for determining riparian restoration potential. *Restoration Ecology* 2:242-246.
- Sheet, K.R., and J.M.H. Hendrickx. 1995. Non-invasive soil water content measurement using electromagnetic induction. *Water Resour. Res.* 31:2401-2409.
- Silliman, S.E., B. Berkowitz, J. Simunek, and M.Th. Van Genuchten. 2001. Fluid flow and solute migration within the capillary fringe. *Groundwater* 1:76-84.
- Simunek, J., T. Vogel, and M.Th. Van Genuchten. 1994. The SWMS-2D code for simulating water flow and solute transport in two-dimensional variably saturated media, V.1.2. Research Rep. No. 132, U.S. Salinity Laboratory, Agricultural Research Service, U.S. Dept. of Agriculture, Riverside, California.
- Simunek, J., M. Sejna, and M.Th. Van Genuchten. 1998. HYDRUS-1D code for simulating the one-dimensional movement of water, heat, and multiple solutes in variably saturated media. IGWMC-TPS 70, Ver. 2.0, International Ground Water Modeling Center, Colorado School of Mines, Colorado.
- Snedecor, G.W., and W.G. Cochran. 1967. *Statistical methods*. 6th ed. The Iowa State Univ. Press, Ames, Iowa.
- Steel, R.G.D., and J.H. Torrie. 1980. *Principles and procedures of statistics. A biometrical approach*. 2nd ed. McGraw-Hill, New York.
- Sterling, J.M. 2000. Spatial distribution of chloride and ^{36}Cl deposition in the conterminous united states. M.S. Independent Study, Hydrology Program, New Mexico Tech.

- Topp, G.C., J.L. Davis, and A.P. Annan. 1980. Electromagnetic determination of soil water content: Measurements in coaxial transmission lines. *Water Resour. Res.* 16:574-582.
- Torres, J.S., and R.J. Hanks. 1989. Modeling water table contribution to crop evapotranspiration. *Irrig. Sci.* 10:265-279.
- Van Genuchten, M.Th. 1980. A closed-form equation for predicting the hydraulic conductivity of unsaturated soils. *Soil Sci. Soc. Am. J.* 44:892-98.
- White, R.E. 1997. *Principles and practice of soil science: The soil as natural resource.* 3rd ed. Blackwell Science, Oxford.
- Wösten, J.H.M. 1987. Description of water retention and hydraulic conductivity curves with analytical functions. Report No. 2019, Soil Survey Institute, Wageningen, The Netherlands.
- Work Group SWAP. 1996. Soil-water-plant model. Dept. of Water Resources. Wageningen Agricultural University, Wageningen, The Netherlands.
- Zwillinger, D. 1996. *Standard mathematical tables and formulae.* 30th ed. CRC Press, Boca Raton, Florida.